Multi-influential interactions alters behaviour and cognition through six main biological cascades in Down syndrome mouse models

Arnaud Duchon, Maria del Mar Muñiz Moreno, Sandra Martin Lorenzo, Márcia Priscilla Silva de Souza, Claire Chevalier, Valérie Nalesso, Hamid Meziane, Paulo Loureiro de Sousa, Vincent Noblet, Jean-Paul Armspach, et al.

Multi-influential interactions alters behaviour and cognition through six main biological cascades in Down syndrome mouse models

Arnaud Duchon[1,2,3,4], Maria del Mar Muñiz Moreno[1,2,3,4], Sandra Martin Lorenzo[1,2,3,4], Márcia Priscilla Silva de Souza[1,2,3,4], Claire Chevalier[1,2,3,4], Valérie Nalesso[1,2,3,4], Hamid Meziane[5], Paulo Loureiro de Sousa[6], Vincent Noblet[6], Jean-Paul Armspach[6], Veronique Brault[1,2,3,4] and Yann Herault[1,2,3,4,5,*]

[1] Institut de Génétique et de Biologie Moléculaire et Cellulaire, department of translational medicine and neurogenetics 1 rue Laurent Fries, 67404 Illkirch Graffenstaden, France

[2] Centre National de la Recherche Scientifique, CNRS UMR 7104, Illkirch Graffenstaden, France

[3] Institut National de la Santé et de la Recherche Médicale, INSERM U964, Illkirch Graffenstaden, France

[4] Université de Strasbourg, Illkirch Graffenstaden, France

[5] Institut Clinique de la Souris (ICS), CELPHEDIA, PHENOMIN, 1 rue Laurent Fries, 67404 Illkirch Graffenstaden, France

[6] Université de Strasbourg, CNRS UMR 7357, ICube, FMTS, Strasbourg, France

*Corresponding author:

Email: herault@igbmc.fr

Keywords: Down syndrome, mouse model, partial trisomy 21, Down syndrome critical region, genotype–phenotype maps, learning, memory, transcriptomic.

Short title: Neuronal altered pathways in Down syndrome mouse models

Highlights

- Brain function and morphology changes in DS mouse models result from multiple genetic loci
- Each combination of loci induces specific alteration of gene expression profile in mouse models
- Altered gene expression converges to a few functional pathwys in DS mouse hippocampi
- The synaptic pathway analysis leads to six connected biological cascades and defines a specific DS disease network

Abstract

Down syndrome (DS) is the most common genetic form of intellectual disability caused by the presence of an additional copy of human chromosome 21. To provide novel insights into genotype–phenotype correlations, we screened the *in vivo* DS mouse library with standardized behavioural tests, magnetic resonance imaging (MRI) and hippocampal gene expression. Altogether this approach brings novel insights into the field. First, we unravelled several genetic interactions between different regions of the chromosome 21 and how they importantly contribute in altering the outcome of the phenotypes in brain function and structure. Then, in depth analysis of misregulated expressed genes involved in synaptic dysfunction highlitghed 6 biological cascades centered around DYRK1A, GSK3β, NPY, SNARE, RHOA and NPAS4. Finally, we provide a novel vision of the existing altered gene-gene crosstalk and molecular mechanisms targeting specific hubs in DS models that should become central to advance in our understanding of DS and therapies development.

Introduction

Down syndrome (DS) is the most common genetic form of intellectual disability and was first described as a disease by John Langdon Down in 1866. One century later, genetic studies demonstrated that DS is caused by trisomy of human chromosome 21 (Hsa21) (1). People with DS have a wide range of phenotypic and physiological features with some phenotypic variability but always present several disabling features like mental retardation or Alzheimer disease (2). The leading cause of DS is non-disjunction of chromosome 21 (3). However, in rare cases, people with partial Hsa21 duplications are observed with a smaller spectrum of DS features. Studying these rare conditions increased our understanding of the genotype–phenotype correlations in DS (4-10). The understanding of DS has been substantially improved over the years. Recently, two human genetic studies showed that not a single trisomic region can be responsible for all DS features but rather several susceptibility regions when

63 presented in 3 copies, in people with partial duplication of Hsa21, can induce a large variety of
64 features (5, 7). Nevertheless, several patients displayed complex rearrangement like contiguous
65 or non-contiguous deletions or duplications, copy number variations of other regions or
66 duplication of genes located in the short arm of Hsa21, that can potentially impact the
67 phenotypic outcome of the Hsa21 duplication and add noise to the genetic dissection of human
68 trisomy 21 clinical manifestations.

69 To circumvent the difficulties in studying DS in human, several efforts have been made
70 to generate DS mouse models (11). Indeed, there are three independent mouse homologous
71 regions to Hsa21, carrying altogether 158 protein-coding homologous genes of the 218 protein-
72 coding genes identified on the Hsa21 (12). The largest region is found on the mouse
73 chromosome 16 (Mus musculus 16, noted as Mmu16) in a fragment of 22.42 Mb with 119
74 orthologous genes between *Lipi* and *Zbtb21* (13). The most telomeric part is splitted into two
75 parts. The first part is found on the mouse chromosome 17 (noted as Mmu17) with 19
76 homologous genes in 1.1 Mb interval between *Umodl1* and *Hsf2bp*. Then, the second part is on
77 the mouse chromosome 10 (Mmu10) with 37 genes included in the 2.3 Mb *Cstb-Prmt2* genetic
78 interval (11, 12, 14). Several DS mouse models have been generated over the years, most of
79 them were carrying trisomy of the largest genetic region located on Mmu16, and have built the
80 *in vivo* DS mouse library (11, 14). The Ts(17^{16})65Dn (noted Ts65Dn) is the most widely used
81 DS model and it is quite unique with a supplementary mini-chromosome obtained by x-ray
82 irradiation of the male germline and containing the centromeric region of Mmu17, with genes
83 from *Psid-ps2* to *Pde10a*, and the 13.5 Mb telomeric fragment of Mmu16 containing genes
84 between *Mrpl39* and *Zbtb21* (15-18). Several models were made by chromosomal engineering
85 (11) and carry segmental duplication of Mmu16. The Dp(16*Lipi-Zbtb21*)1Yey (noted Dp1Yey)
86 corresponds to the duplication of the entire Mmu16 region syntenic to Hsa21 (19). The
87 Dp(16Cbr1- Fam3b)1Rhr (noted Dp1Rhr) model carries a duplication from *Cbr1* to *Fam3b* and
88 demonstrate the contribution of the DS critical region (DCR) (20-23). All the DS mouse models

displayed defects in behaviour and cognition which had been investigated in different laboratories with different protocols and environmental condition making difficult inter-model comparison (11).

In order to improve our knowledge on DS, we analysed six DS mouse models, that carries either large segmental duplication, like the Dp1Yey, or transgenic line overexpressing *Dyrk1a*, the main driver gene of DS phenotype found on the Mmu16 (24-28). We used a unique and in depth behaviour, morphological and transcriptomics pipeline in adult animals to dissect the contribution of the genes located on Mmu16 to DS mouse features. The behaviour pipeline relied on assessing specific hippocampal-dependent brain functions found altered in people with DS (29, 30). Thus, we performed standardized tests for the Y-maze, Open field (OF), Novel Object Recognition (NOR), Morris Water Maze (MWM) and contextual and cue Fear Conditioning (FC). All procedures were carried in similar environmental conditions to reduce any impact (31, 32). Besides, variations in specific brain regions have been observed in people with DS and mouse models (33-36). Neuroanatomical changes affect the whole brain volume or specific regions like the frontal region of the limbic lobe or the hippocampus in people with DS. Thus, we performed an in depth morphological investigation of the brain by magnetic resonance imaging (MRI). Finally, whole gene expression was performed on hippocampi isolated from the six models to decipher the genes, functional pathways and biological cascades affected in the different DS mouse models.

Material and Methods

Mouse lines

The duplications of different Mmu 16 regions (Dp(16*Lipi-Zbtb21*)1Yey (or Dp1Yey), the Dp(16*Hspa13-App*)3Yah (noted Dp3Yah), the Dp(16*Cbr1- Fam3b*)1Rhr (or Dp1Rhr)) and the BAC transgenic for *Dyrk1a* (Tg(*Dyrk1a*)) models were previously described (19, 20, 24, 37). The genetic background of the DS lines carrying each duplication was pushed toward the

C57BL/6J (B6J) genetic background for more than 7 generation of backcross. The only exception is the trisomic Ts65Dn (Ts(17^{16})65Dn) mice, initially obtained from the Jax, that was kept on a F1 B6C3B genetic background (with the C3B line as a C_3H/HeH congenic line for the BALB/c allele at the *Pde6b* locus (38)). The Dp(16*Cyyr1*-*Clic6*)5Yah (noted Dp5Yah) was generated by the *in vivo* TAMERE technology inserting loxP sites in *App* and *Runx1* (see Supplementary information). In the Dp3Yah and Dp5Yah models, only 2 complete copies of *App* and *Runx1* genes are expressed. The Dp5Yah line was crossed with the Dp1Rhr in order to generate the Dp5Yah/Dp1Rhr (also noted Dp5/Dp1) coumpound transheterozygote carrying a similar trisomic Mmu16 gene content to that of the Ts65Dn. Indeed, only 15 Hsa21 homologous genes (*Mrpl39, Jam2, Atp5j, Gabpa, App, Cyyr1, Runx1, Setd4, Mx2, Tmprss2, Ripk4, Prdm15, C2cd2 and Zbpb21*) over 174 are not in 3 copies in Dp5/Dp1 compared to Ts65Dn. In addition 46 protein-coding genes located on the Mmu17 centromeric region in the Ts65Dn minichromosome (13, 16) are not trisomic in the Dp5/Dp1. The Dp5Yah model was also combined with the Tg(*Dyrk1a*) by crossing Dp5Yah/+ and Tg(*Dyrk1a*)/0 animals and generating the four genotypes (Dp1Yah, Dp5Yah, Tg(*Dyrk1*a) and [Dp5Yah; Tg(*Dyrk1a*)] noted here Dp5-Tg), to test specific interaction between Dp5Yah and *Dyrk1a* overdosage.

All the lines were maintained under specific pathogen-free (SPF) conditions and were treated in compliance with the animal welfare policies of the French Ministry of Agriculture (law 87 848) and the phenotyping procedures were approved by our local ethical committee (Com'Eth, n°17, APAFIS n°2012-069).

Behaviour pipeline

A serie of behavioural experiments were conducted in mice with a range of age starting at 2,5 up to 7 months for the last test, as described in the Supplementary information. The tests were administered in the following order: Y-maze, open field, novel object recognition (24h), Morris water maze and fear conditioning (contextual and cue). Behavioural experimenters were blinded to the genetic status of the animals. Separate groups of animals were composed for each

line (as indicated in S1 table). Several mouse models found defective for the NOR performed with 24h of retention memory were also tested after 1h of retention. The Dp5Yah crossed with Tg(*Dyrk1a*) was tested for Y-maze and NOR at 24h. All the standard operating procedures for behavioural phenotyping have been already described (39-43) and are detailed in the supplementary information.

Magnetic Resonance Imaging

A dedicated cohort of animals at the age 102 +/- 7 days was anesthetized and perfused with 30 ml of room temperature 1X Phosphate Buffer Saline (PBS) complemented with 10% (% w/v) heparine and 2mM of ProHance Gadoteridol (Bracco Imaging, Courcouronnes, France) followed by 30ml of 4% PFA complemented with 2mM of ProHance Gadoteridol. Then the brain structure was dissected and kept in PFA 4% 2mM ProHance over night at 4°C. The next day, each specimen was transferred into 1X PBS 2mM ProHance until imaging.

Just prior to imaging, the brains were removed from the fixative and placed into plastic tubes (internal diameter 1 cm, volume 13 mL) filled with a proton-free susceptibility-matching fluid (Fluorinert® FC-770, Sigma-Aldrich, St. Louis, MO). Images of excised brains were acquired on a 7T BioSpec animal MRI system (Bruker Biospin MRI GmbH, Ettlingen, Germany). Images were reconstructed using ParaVision 6.0. An actively decoupled quadrature-mode mouse brain surface coil was used for signal reception and a 72-mm birdcage coil was used for transmission, both supplied by Bruker. The first protocol consisted of a 3D T2-weighted rapid-acquisition with relaxation enhancement (RARE). The second imaging protocol consisted of a 3D T2*-weighted Fast Low Angle (FLASH) sequence. The image matrix for both sequences was 195 x 140 x 90 over a field of view 19.5 x 14.0 x 9.0 mm^3 yielding an isotropic resolution of 100 μm and was treated and analysed for anatomical parameters as detailed in the supplementary information.

166 **Gene expression assay**

167 Hippocampus were isolated from DS trisomic models and their littermate controls (N =
168 5 per group) and flash frozen in liquid nitrogen. Total RNA was prepared using the RNA
169 extraction kit (Qiagen, Venlo, Netherlands) according to the manufacturer's instructions. The
170 samples quality was checked using an Agilent 2100 Bioanalyzer (Agilent Technologies, Santa
171 Clara, California, USA). Gene expression analysis was carried out using GeneChip® Mouse
172 Gene 1.0 ST arrays (Affymetrix, Santa Clara, CA). All the procedure and the analysis are
173 detailed in the supplementary information. Raw microarray data and re-analysed data have been
174 deposited in GEO (Accession No. GSE149470).

175

176 **Bioinformatic analysis**

177 The gene expression profile of the mouse hippocampi isolated from Dp1Yey, Dp3Yah,
178 Ts65Dn, Dp5/Dp1, Dp5Yah, Dp1Rhr and Tg(*Dyrk1a*) trisomic mouse models was analysed
179 with a specific bioinformatic pipeline and controlled for quality prior and after the data pre-
180 processing and normalization (see supplementary information in the detailed material and
181 methods section). The identification of the differentially expressed genes (DEGs) was
182 performed using a method based on fold change rank ordering statistics (FCROS)(44). In the
183 FCROS method, k pairs of test/control samples are used to compute fold changes (FC). For
184 each pair of test/control samples, obtained FCs for all genes are ranked in increasing order.
185 Resulting ranks are associated to genes. Then, the k ranks of each gene are used to calculate a
186 statistic and resulting probability (f-value) used to identify the DEGs after fixing the error level
187 at 5% False Discovery Rate (FDR).

188 We performed the functional differential analysis using GAGE (45) and grouped all the
189 pathways into 8 functional categories (noted meta-pathways). The functional intermodel meta-
190 pathway connectivity was studied identifying the genes shared between pathways and models
191 inside the same meta-pathway. Then, to assess the gene connectivity we build a minimum fully

connected protein-protein interaction (PPI) network (noted MinPPINet) of genes known to be involved in synaptic function as they were associated with synaptic pathways via GO (46) and KEGG databases (47) and furthermore added regulatory information to build the final RegPPINet. We used the betweenness centrality analysis to identify hubs, keys for maintaining the network communication flow. The relevance of the connecting nodes was further predicted by the machine learning algorithm Quack (48). Finally, we computed 100000 random networks with a similar degree, to assess if the likelihood of observing such connectivity in the DS network was more than one can expect by chance using statnet and sna R packages (https://cran.r-project.org/web/packages/statnet/index.html; https://cran.r-project.org/web/packages/sna/index.html).

Western blot

The expression levels of the RHOA protein and Myosin Light Chain phosphorylation by Myosin Light Chain Kinase part of the RHOA pathway were analysed using Western Blot in 5 animals Dp1Yey and 5 control (wt) littermates (See Fig 4G, Supplementary fig 16, and supplementary information). We used the following primary antibodies: anti-RHOA (2117, Cell Signaling, USA, 1:1.000), anti-pMLC (Thr18/Ser19 #3674, Cell signalling, Boston, MA, USA, 1:1.000) and mouse monoclonal Anti-β-Actin−Peroxidase antibody (A3854 Sigma, 1:150.000); and HRP conjugated Goat anti-Rabbit IgG secondary antibody (A16096, Invitrogen, France). Protein signals were visualized with Amersham™ Imager 600 and were quantified using ImageJ and the statistical analysis using Sigma Plot. The relative amount of RHOA and p-MLC proteins was calculated as the ratio of the signal detected for each proteins of interest compared to the β-actin signal detected and normalized by the mean signal of the wt samples.

Visual stimulation

Mice raised in a standard light cycle were housed in constant darkness for two weeks. Then, animals in the light-exposed condition group, were consecutively exposed to light for 0, 1, 3, or 7.5 h before being sacrificed. Instead, animals part of the dark-housed condition group were sacrificed in the dark. After euthanasia, their eyes were enucleated before the visual cortex dissection in the light and flash frozen in liquid nitrogen. cDNA and quantitative PCR were performed as indicated in the supplementary information. The Ct values were transformed to quantities by using the comparative Ct method. Hence, all data were expressed relative to the expression of the most expressed gene. This relative expression levels, were normalized with Genorm by keeping the more stable reference genes (49). To calculate fold-induction, relative quantity of gene expression at each time point was divided by the mean of relative level of gene expression of dark housed mice for corresponding genotype. The mean and standard error were calculated at each time point from these fold-induction values.

Statistical analysis

All data are expressed as mean group value ± standard error of the mean (SEM) or as box plots with the median and quartiles. For each data set, we analysed if the data was normally distributed by Shapiro–Wilk test and Quantile-Quantile plots (S2 Fig) and the homogeneity of variances by the Brown-Forsy test. Differences between groups were inferred by one-way ANOVA (Open field) and ANOVA for repeated measures, or in case of datasets where the assumptions of normality or homogeneity of variances were not fulfilled we performed the Kruskal-Wallis non-parametric test. The post hoc tests (Fisher LSD Method) were conducted only if the F parameter in ANOVA achieved 0.05 level. All the behavioral analysis results are found in S1 table. For MRI data, intergroup comparisons on region-based data were conducted on the normalized volumes (i.e., ratio between the volume of the structure and the whole brain volume) of each segmented structure using the Student t-test while correcting by multiple testing setting up a FDR correction.

Results

Dissecting the contribution of Mmu16 subregions to the DS-related behavioral phenotypes in mouse models

We wanted to dissect the contribution of sub-regions located in the telomeric part of *Mus musculus* chromosome 16 (Mmu16), homologous to Hsa21 (50), to the DS-related cognitive phenotypes. First, we selected 4 DS mouse models: the Ts65Dn, the most commonly used DS model (15), and three additional models that are carrying segmental duplications of well-defined sub-regions located on the Mmu16, the Dp1Yey (19), Dp3Yah (37) and Dp1Rhr (20). In addition, we engineered a new one, the Dp5Yah, corresponding to three functional copies of the genes included in the genetic interval between *Cyyr1* to *Clic6*. This model was crossed with the Dp1Rhr one in order to generate the Dp5Yah/Dp1Rhr (noted Dp5/Dp1) coumpound transheterozygote carrying a trisomic gene content similar to the Ts65Dn for the genes located on the Mmu16. We also included a model carrying an additional copy of *Dyrk1a*, one of the driver genes for DS-related phenotypes (25, 35), and the Tg(*Dyrk1a*) combined with Dp5Yah model (noted Dp5-Tg) (S1 Fig). We used standardized behavioral tests to study several aspects of learning and memory in mice including the Y-maze (working memory), the open field (exploration memory), the novel object recognition (recognition memory), the Morris water maze (spatial memory) and the fear conditioning (associative memory). For all the lines, independent cohorts of control and trisomic mouse littermates went through the pipeline at similar ages, then the resulting data were processed using standard statistical analyses (See supplementary information for details). First, we assesed the potential existence of a background effect over the distribution of the measurements taken in the different tests. In our condition the Q-Q plots with the cumulative frequency were linear and thus, no notable

difference between B6J or hybrid B6JC3B wild-type controls was observed (see Fig 1, S1 table, S2 Fig).

Mice activity and working memory were evaluated in the Y-maze (Fig 1A). The number of arm entries in the Y-maze showed that only Tg(*Dyrk1a*) mutant line was hyperactive in this test while deficit in spontaneous alternation was found in Dp1Yey (51), Ts65Dn (52), Dp1Rhr and Tg(*Dyrk1a*) (53). The Dp5/Dp1 also showed a clear deficit in the percentage of spontaneous alternation as compared to littermate controls while Dp5Yah trisomic animals showed normal performance.

The patterns of exploratory activity and anxiety were assessed in the open field (Fig 1B). Ts65Dn, Tg(*Dyrk1a*) and Dp5-Tgpresented hyperactivity with an increased travelled distance compared to wild-type littermates, and support, for Tg(Dyrk1A), results obtained in the Ymaze. In addition, Ts65Dn mice displayed thigmotaxic behavior with incraesed distance travelled at the periphery.

The spatial reference memory was tested in the standard Morris water maze (MWM) task, in which mice have to escape from a circular pool of opaque water by localising a hidden platform at a single fixed location using distal spatial cues. We analysed the velocity, the distance travelled by the mice to reach the platform and the thigmotaxis over training (S3 Fig). The velocity of Dp1Yey and Dp5Yah, was slightly lower than the wild-type mice (S3 FigB). As previously described (22, 54-60), Ts65Dn mice displayed a longer distance travelled to find the platform during all the sessions, compared to the wild type (S3 FigA). Although Tg(*Dyrk1a*) were able to locate the platform, they also showed delayed acquisition compared to the control mice. Surprisingly, the Dp1Yey, Dp1Rhr, Dp5Yah and Dp3Yah completed this test without any difference with the wild type group. Retention of place location was evaluated during a single probe trial (PT) with no platform available, 24h after the last training session (Fig 1D). The results confirmed as previously shown, that all the mouse strains except the Ts65Dn, remembered where the platform was located after the learning sessions. Interestingly, the

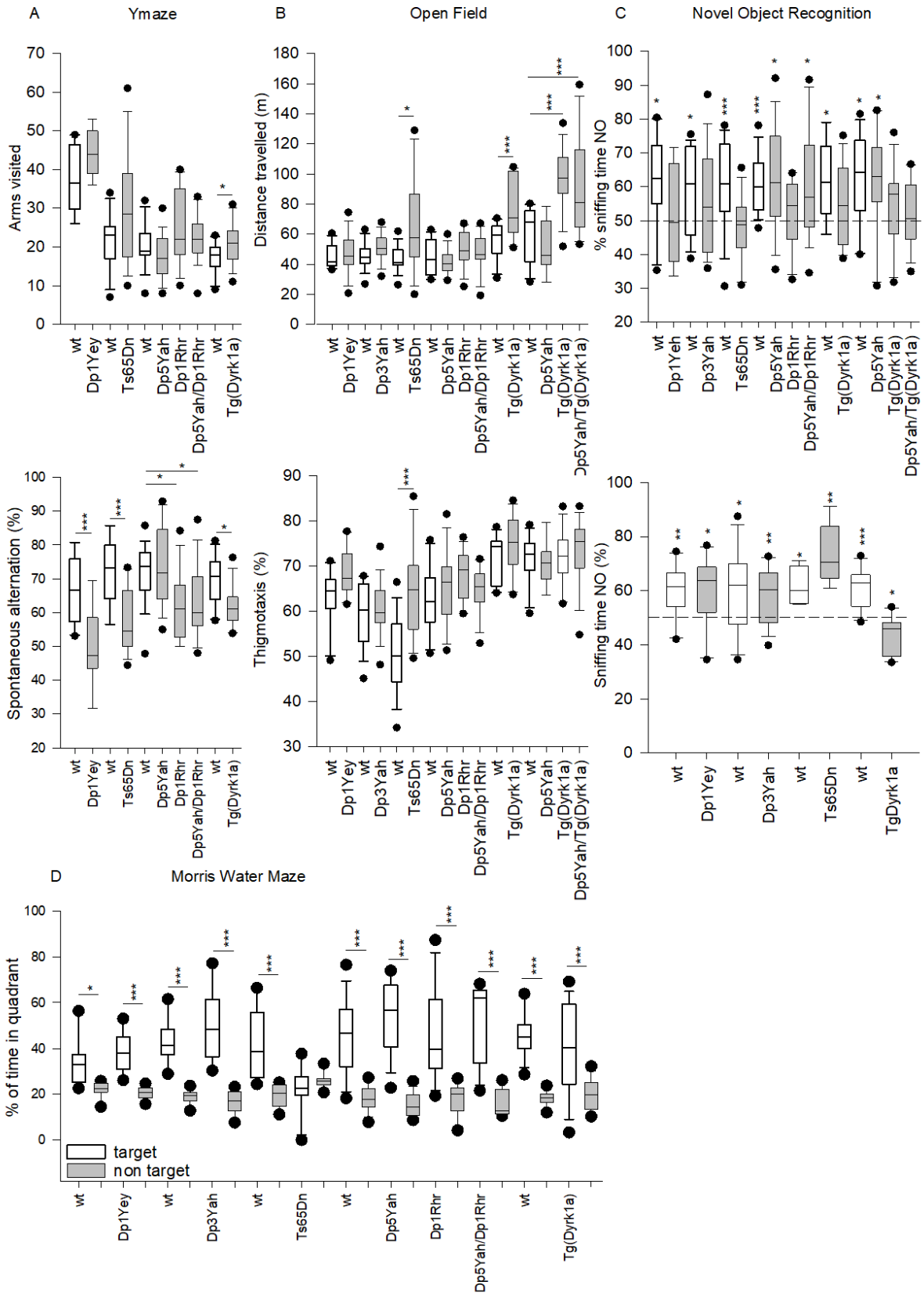

Figure 1. Standardized behavioural profiling of DS mouse models.
Y-maze spontaneous alternation. Arm visited (A upper panel) and alternation rate (A lower panel) are presented as box plots with the median and quartiles (upper and lower 90% confidence interval are indicated by a grey box). Only the Tg(*Dyrk1a*) mice were showed

hyperactivity in this test with increased arms entries compared to the wild type (p=0,017). Alternation rate in Dp1Yey (p=0,002), Ts65Dn (p<0,001), Dp1Rhr (P=0,012), Dp5/Dp1Rhr (p=0,018) and Tg(*Dyrk1a*) (P=0,010) mice was significantly lower than respective wild-type mice. Exploratory activity in a novel environment. Distance travelled (B upper panel) and % of distance travelled in peripheral zone recorded in the Open field arena (B lower panel). The total distance travelled was significantly higher in Ts65Dn (p=0,022), Tg(*Dyrk1a*) (p=0,008) and Dp5Yah/Tg(*Dyrk1a*) (p>0,001). Moreover, the % of distance in the peripheral zone was increased in Ts65Dn (p>0,001) mice comapred to wild type mice. Novel Object Recognition with 24 hour (C upper panel) or 1 hour retention time (C lower panel). The results are presented as % of sniffing time (as box plots with the median and quartiles) for the novel object (NO). For 24 hours time laps, one sample t test vs 50% (hazard) showed that Dp1Yey (p=0,837), Dp3Yah (P=0,173), Ts65Dn (p=0;432), Dp1Rhr (p=0,492), Tg(*Dyrk1a*) (p=0,144) and Dp5Yah/Tg(*Dyrk1a*) (P=0,488) failed to recognize the new object. The Dp5Yah genomic fragment restored the capacity of the Dp1Rhr in the Dp5Yah/Dp1Rhr mice (p=0,0157). For 1 hour retention time, all the mice were able to discriminate the NO except for the Tg(*Dyrk1a*) (p=0,011 preference for FO). Probe test session in Morris Water Maze (D). The results are presented as % of time in the target quadrant. All the mice have spent more time in the target quadrant versus non target excepted for the Ts65Dn mice (p=0,398) (* p<0.05, **p<0.01, ***p<0.001).

Ts65Dn model, and to a lower extend the Tg(Dyrk1a) one, presented marked thigmotaxic behaviour, spending higher percentage of time in the peripheral zone as compared to controls (S3 FigC). Finally, to check the visual ability of mice, we performed a visual training version of the MWM during which the platform postion is indicated by a flag. All mice were able to find the visible plateform without any significant difference with controls except for the Tg(*Dyrk1a*) that presented a small delay in session 2 (S3 FigA).

We then evaluated non-spatial recognition memory using the novel object recognition (NOR) paradigm with the retention time of 24h. The percentage of sniffing time for the novel object was analysed and compared to 50% (hazard). This analysis showed that Dp1Yey, Dp3Yah, Ts65Dn, Dp1Rhr and Tg(*Dyrk1a*) were not able to discriminate the familiar and the novel objects unlike the Dp5Yah and more surpringly the Dp5/Dp1 (Fig 1C). to further characterize the effect/lack of effect of Dp5Yah mutation on n ovel object recognition, the Dp5Yah mouse line was crossed with the Tg(*Dyrk1a*) and compared to new sets of wild-type, Dp5Yah and Tg(Dyrk1a) mice . Interestingly, we found that the Dp5Yah/Tg(*Dyrk1a*) and as expected the Tg(*Dyrk1a*) displayed altered novel object discrimination while the Dp5Yah spent

more time exploring the novel object than the familiar one. We also assessed Dp1Yey, Dp3Yah, Ts65Dn and Tg(*Dyrk1a*) short term memory performing the NOR with 1 hour delay between acquisition and retention and only the Tg(*Dyrk1a*) mice showed a deficit.

All the trisomic lines were also tested for associative memory in the Pavlovian fear conditionning test. All the groups showed higher percentage of freezing during the 2 min post-shock compared to the habituation session, indicating that all groups developped fear responses during the training session (S4 Fig). When animals were re-exposed 24 h later to the same context, the level of freezing in all groups was increased compared to the habituation (PRE2 and PRE4). However, freezing time for Ts65Dn mice was lower compared to the respective control littermates. When we assessed cued fear conditioning in a new context, all the mice presented an increased time of immobility with a strong difference between pre-cue and cue periods (S4 Fig). In addition, Dp1Yey and slightly Ts65Dn showed lower freezing during presentation of the cues as compared to wildtype counterparts. These data suggest altered emotional associative memory Ts65Dn.

Dissecting the contribution of Mmu16 sub-regions to the DS-related brain morphological phenotypes in mouse models

DS models have been reported to show brain morphological alterations of specific regions (35). Thus, we wondered If we could detect changes in the brain morphology using MRI on these different partial trisomic mice models. Data were first analyzed using a volume approach and a brain region atlas. We confirmed that the brain of Tg(*Dyrk1a*) mice was larger ($p<0,001$) (35) and the brain of Dp1Yey mice was smaller than the respective wildtypes. Then, we analyzed different brain regions/structures taking into consideration/correction the whole brain volume. Even with this correction, the Tg(*Dyrk1a*) mice were the most affected in terms of the brain structures volume, and on the contrary, the Dp1Rhr mice did not show any significant variation compared to the wt mice. Several regions, such as the basal forebrain

361 septum, central gray matter, the rest of midbrain, and superior colliculi were significantly larger
362 in Tg(*Dyrk1a*), Ts65Dn and Dp1Yey DS models. Moreover, the cerebellum, hypothalamus,
363 inferior colliculi and caudate putamen were significantly different in Dp1Yey and Tg(*Dyrk1a*)
364 compare to the control group (S2 table, S5 Fig) and a few additional areas were altered
365 specifically in certain models (Amygdala, Globus pallidus, Hippocampus, Neo Cortex, and
366 Thalamus for Tg(*Dyrk1a*); External capsule, Fimbria, and Ventricles for Dp1Yey). Altogether
367 this brain morphometric analysis showed a greater similarity between Dp1Yey and *Dyrk1a*
368 overexpression transgenic models with intermediate overlapp with the Ts65Dn mouse model.
369
370 **Dissecting the contribution of Mmu16 subregions to the DS-related transcriptome profiles**
371 **in mouse models**
372 Various studies have shown the consequences of trisomy on gene expression (61-70).
373 Here we took the opportunity to dissect the alteration of gene expression and functional
374 pathways in various DS trisomic models carrying different duplications of the Mmu16. We
375 analyzed the Ts65Dn, Dp1Yey, Dp3Yah, Dp5/Dp1, Dp5Yah, Dp1Rhr, and we included the
376 trisomic model for *Dyrk1a* alone, Tg(*Dyrk1a*). Considering the hippocampal formation as a hub
377 structure involved in learning and memory, we performed gene expression analysis in the adult
378 hippocampus comparing the DS models with their own littermate controls using a unique
379 pipeline for all the models. For each DS model, we defined the expressed genes (noted as EGs)
380 as the genes whose expression level was detected, the differentially expressed genes (noted as
381 DEGs) as the genes whose expression level was found to be significantly altered in the trisomic
382 model compared to the controls littermates, and then the trisomic expressed genes (TEGs) as
383 the DEGs that are included inside the duplicated chromosomal regions for each model (S3 table,
384 Table 1).

Mouse lines	Dp1yey	Dp3Yah	Ts65Dn (Mmu16)	Dp5/Dp1	Dp5Yah	Dp1Rhr	TgDyrk1A	Ts65Dn (Mmu17)
Nb of probes detected by the array					35556			
Nb of annotated probes detected (without control probes)					27359			
Number of trisomic genes detected by the array	155	21	130	127	87	40	1	40
Differential expressed genes (DEGs)	711	826	1074	922	736	1306	850	
Differential expressed trisomic genes (DETGs)	66	13	64	54	39	18	1	28
% of **DETGs	43%	62%	49%	43%	45%	45%	100%	70%
% of compensated trisomic genes detected	57%	38%	51%	57%	55%	55%	0%	
Number of GAGE KEGG and GOs (CC,BP,MF) terms disregulated in the trisomic model FDR<0.1	244	67	12	111	318	225	231	
Number of GAGE KEGG and GOs (CC,BP,MF) terms **upregulated** in the trisomic model FDR<0.1	207	60	3	33	4	132	222	
Number of GAGE KEGG and GOs (CC,BP,MF) terms **downregulated** in the trisomic model FDR<0.1	37	7	9	78	314	93	9	
Number of GAGE KEGG and GOs (CC,BP,MF) terms in the trisomic model unique to each mice line FDR<0.1	80	1	2	30	195	107	64	

*DEGs/DETs: Diferential expressed genes/ Diferential expressed
**DETGs/DETTs: Diferential expressed trisomic genes/

Table 1. Differential expression analysis results of the seven models analysed. DEGs are Differential Expressed Genes and TEGs for Differential Expressed trisomic genes. * Analysis done with Mmu17 and 16 trisomic genes. GO are Go functional terms involved in cellular compartment (CC), molecular function (MF) and biological processes (BP).

Although most of the genes in 3 copies were overexpressed in the relevant mouse model-derived hippocampi with a ratio around 1.5 (S6 Fig), from 38% to 57% of the trisomic genes showed a dosage compensation (Table 1, S3 table). While this compensation is expected, we noticed that most of the compensated genes behave similarly in the different trisomic context, even if the experiments were done independently. As such the genes from *Cldn17* to *Krtap11-1*, including the keratin cluster were not overexpressed when trisomic in any model (Dp1Yey, Ts65Dn, Dp5/Dp1 or Dp5Yah). This could be due to the fact that this region seems to be under strong regulatory constrains as on the borders two REST sites plus a LaminB1 peak encompassing this region were found (UCSC browser), while *Btg3* (*BTG Anti-Proliferation Factor 3*) and C21orf91 (*Chromosome 21 open reading frame 91*, also known as *D16Ertd472e*), or *Mrpl39 (Mitochondrial Ribosomal Protein L39), Jam2 (Junctional*

Adhesion Molecule 2), Atp5J (ATP synthase peripheral stalk subunit F6), Gabpa (GA binding protein transcription factor subunit alpha) and *App (amyloid beta precursor protein)* are overexpressed in various DS models. We also found that the genes located on the trisomic segment not homologous to Hsa21 on the Mmu17 in Ts65Dn hippocampi, were overexpressed (S7 Fig). This was also observed in the Ts65Dn heart in a previous study (16). Looking in detail into the homologous Hsa21 region in Mmu17, we saw two main genetic effects due to the overdosage of the Mmu16 region homologous to Hsa21. Noticeably, *Cbs*, coding for the Cystathionine beta-synthase, another driver gene for DS cognitive phenotypes (71), was found down-regulated in all the models, except Dp3Yah and Tg(*Dyrk1a*); suggesting a direct control of the *Cbs* transcription by at least two loci, one located in the Dp5Yah, and another one, not due to *Dyrk1a* overdosage, in the Dp1Rhr trisomic region. Similarly, under-expression of the *glucagon like peptide 1 receptor (Glp1r)* was observed in Dp1Yey, Ts65Dn, Dp5/Dp1 and Dp5Yah. Oppositely, this gene was overexpressed in Dp1Rhr and not affected in Tg(*Dyrk1a*).

Here too, *Dyrk1a* dosage was not involved, but at least two loci controlling *Glp1r* expression with opposite and epistatic effects should be found respectively in the Dp5Yah and Dp1Rhr genetic intervals. Thus a complex genetic interaction took place between different loci and controlling subsequent gene expression.

The analysis of DEGs in each model separately highlighted the capabilities to separate the trisomic individuals from the wild-type littermates (Fig 2A) by principal component analysis (PCA), t-SNE (Fig 2B) or OPLS techniques (See supplementary information). A genome-wide misregulation was found independently of the model, as DEGs were spread in all the chromosomes (S3-S4 tables, S8 Fig), as shown previously (67), although with a stronger impact of the Dp1Rhr duplication on the number of total DEGs detected. The most overexpressed genes in terms of log2 fold change (log2FC) of expression and significance in various genetic conditions were visualised using Volcano plots (S9 Fig, S4 table). For example,

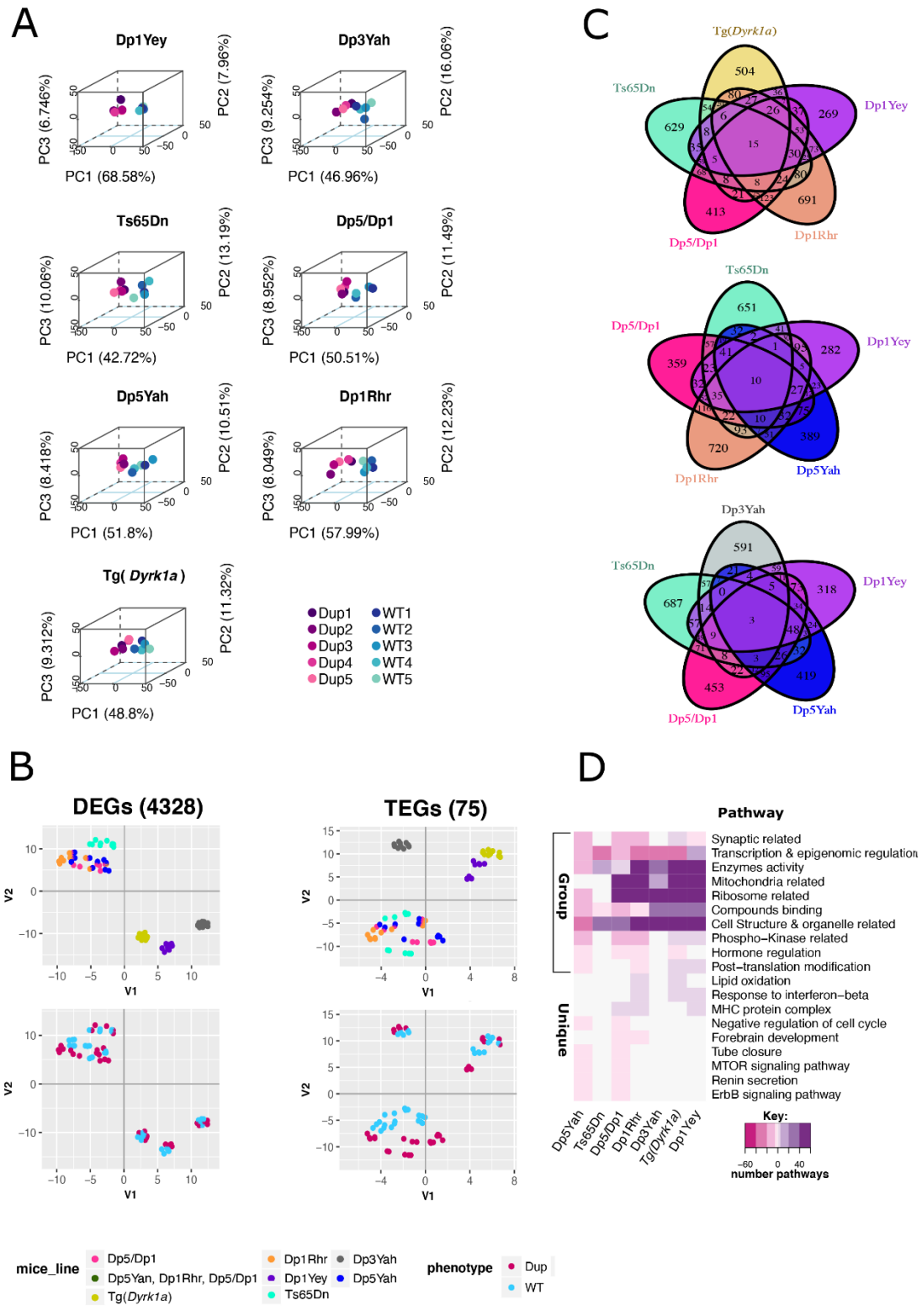

Figure 2: The differential expression analysis discriminates trisomic from disomic hippocampi and identifies common dysregulared genes and pathways. (A) 3D-PCA on the DEGs for each sample allows to separate trisomic (Dp) from disomic (wt) adult hippocampi. B) Left column: two dimensional Principal Component Analysis (2D-PCA) on the 5599 transcripts of the 4328 DEGs over all the samples identified using fcros 0.025<α<0.975. Right column: 2D-PCA on the 75 trisomic genes with a measured expression in all the models. (C) Venn Diagrams showing the overlap in gene expression between the different mouse lines represented in different colours. (D) Heatmap representation of the number and regulation sense

of the pathways shared at least by two mice lines identified using the genome expression for each mice line by GAGE R package and filtered by q-value cut off < 0.1. Grouped in the categories showed on the ordinate: synaptic related, synaptic related: representation of the pathways involved in Myelin sheath and SNARE complex formation, synaptic related: all the synaptic related pathways excluding myelin sheath and SNARE complex formation, Transcription & epigenomics regulation, Enzymes activity, Ribosome related, Mitochondria related, Cell Structure & organelle related, Phospho-kinase related… The color key breaks represents the number of pathways within the categories 60,40,20,5,0.5. The minus or pink color represents down regulated pathways, the white color represents no pathway found in the category and the purple or positive numbers stands for up regulated pathways respectively.

the *listerin E3 ubiquitin protein ligase 1* (*Ltn1*) gene, coding for a major component of the ribosome quality control and causing neurodegeneration in mice (72), was found overexpressed in Dp1Yey, Ts65dn, Dp5/Dp1, and Dp5Yah or *Ifnar2*, coding for the Interferon Alpha and Beta Receptor Subunit 2, is overexpressed as expected in models that carry three copies of this gene (Dp1Yey, Ts65Dn, Dp5/Dp1 and Dp5Yah). Instead, a more controlled gene like the *neuronal acetylcholine receptor subunit alpha-3* (*Chrna3*), is found upregulated only in Dp1Rhr and Dp1/Dp5, certainly due to the overexpression of one gene from the *Cbr1- Fam3b* region but not *Dyrk1a*. Nevertheless, when we performed the intersection between the list of DEGs from the different models, we only found a few genes in common (Fig 2C, S4 table). We decided to combine the analysis of all the lines together using PCA and t-SNE and revealed a strong clustering of models that share the same number of trisomic genes (Fig 2B). t-SNE analysis, based on 4328 DEGs, adding all DEGs detected in each mouse model together, showed different contribution of the various DS models to the transcriptome variation (Fig 2B, left panel) with 2 distinct groups: one encompassing four overlapping trisomies: Ts65Dn, Dp5/Dp1, Dp5, Dp1Rh and three isolated models: Dp1Yey, Dp3Yah and Tg(*Dyrk1a*) that are closer together although Dp3Yah is clearly farthest from the other two. Similar distinct groups were seen when analysing the TEGs (Fig 2B, right panel) and overall, the trisomic and the wild-type individuals in each mouse line were nicely separated. As expected, the expression level of the TEGs and the DEGs in the different trisomic conditions were strongly correlated (S10 Fig). Interestingly, the 4328 DEGs showed a level of mis-regulation strongly correlated between

Dp1Yey and Dp3Yah (33%), Dp5/Dp1 (50%), Dp1Rhr (40%) and Tg(*Dyrk1a*) 42%. Of the 75 TEGS, the correlation was quite strong between Dp1Yey and Tg(*Dyrk1a*) with 28%. Thus, the correlation in gene deregulation showed that *Dyrk1a* overdosage is a key driver of transcriptome deregulation in the Dp1Yey and Dp1Rhr models. Unexpectedly, the correlation of DEGs mis-expression level was lower between Ts65Dn and Dp1Yey (29%) or Dp1/Dp5 (28%). On the opposite, a high number of TEGs are mis-regulated in the same way between Ts65Dn and Dp1Yey (49%) or Dp1/Dp5 (52%; S10 Fig) suggesting that the other region found in 3 copies in the Ts65Dn over Mmu17 must be affecting the general DEGs landscape. We confirmed by qPCR the mRNA overexpression of first, *Dyrk1a* and *Sod1* genes in the DS models where they are trisomic; second, of *Synaptojanin2* and *T lymphoma invasion and metastasis inducing gene 2* that are located on the Mmu17 centromeric region in the Ts65Dn and third, of *Cholinergic Receptor Nicotinic Alpha 1 Subunit (Chrna1)* a gene misregulated in Dp1Yey,Dp5/Dp1, Dp1Rhr and Ts65Dn models (S15 fig). As expected *Cbs*, expression was down regulated in all the models except Tg(*Dyrk1a*) and Dp3Yah. We also detected alterations of the expression of immediate early-response genes *Arc*, *FosB*, *Fos* and *Npas4* that are important for cognition.

Differential functional analysis unravel a few common altered pathways in DS models

To go further, we performed a differential functional analysis and found 12 to 318 mis-regulated pathways in the DS models (table 1, S5 table). Interestingly, the regulation of pathways is trisomic region-dependent, as the Dp5Yah (99%) region produced an overall downregulation whereas the Dp3Yah (89.5 %) and Dp1Rhr (56 %) regions together with the full Hsa21 syntenic model Dp1Yey (84.8 %), an upregulation. To facilitate the understanding, we clustered the broad functional dysregulation into 8 major functionality groups or meta-pathways. We found ribosomal components and mitochondrial processes pathways altered in all models with a high number of intermodel shared genes (S12 Fig). Others meta-pathways

like cell structure and organelles, transcription and epigenetic regulation, interferon and synaptic pathways were more affected in some models than in the others (S13 and S14 Fig). As such, we observed strong and connected effects in the control of transcription and epigenetic regulation, enzyme activity and cell structure and cellular organelles involved in membrane and protein processing (endoplasmic reticulum, Golgi body, lysosome, peroxisome,…; Fig 2D) in the Dp1Yey, Dp5/Dp1, Dp1Rhr, and Tg(*Dyrk1a*) models, whereas the myelinization and 10 SNARE components, such as the *Synaptosome Associated Protein gene 25 and 23* (*Snap25* and *Snap23),* were specifically dis-regulated in the Dp1Yey Dp5Yah and Tg(*Dyrk1a*) models.

Interestingly, we saw a high number of shared genes between these pathways and the models giving rise to a high intermodel pathway connectivity. To assess the gene connectivity & cross talk, we build a protein-protein interaction (PPI) network of genes involved in synaptic function (noted MinPPINet) and furthermore we added regulatory PPIs to build the final RegPPINet. Then, we analysed the betweenness centrality to identify hubs, keys for maintaining the network communication flow that are most susceptible to targeted drugs attacks and the main signalling cascades affected. The relevance of the connecting nodes unknown to play a role in brain dysfunction, was further predicted by the machine learning algorithm Quack[118] and we found several evidences linking 449 (22 with a high confidence score) DEGs to GO/KEGG pathways involved in brain dysfunction, not previously known (S5 table). In fact, several evidences make us consider that those genes should be included in the pathways:gene associations. Inside the evidences we can point that these DEGs were found dis-regulated in hippocampus, were included in the network built by STRING[73] as connecting nodes (not seeds) to produce a fully connected DS network, and their relevance to brain dysfunction was also predicted by Quack, in some cases, with a high score.

Looking into the DS synaptic MinPPINet (Fig 3A), first we analysed the DS network topography and betweenness connectivity and found hubs and genes more central for the

network information flow. As expected from a PPI biological network, after computing 100000 random networks with a similar degree, the likelihood of observing such connectivity in the DS network was more than one can expect by chance (P-value < 2e-16) and it showed a small world effect and scale-free topology. Using a network decomposition approach (see supplementary information), we highlighted 6 major subnetworks or biological cascades that strongly centralized 6 different proteins: DYRK1A, GSK3B, NPY, RHOA, SNARE and NPAS4 proteins (Fig 3B-C). Here, ten genes from the SNARE complex were dysregulated, from those, we validated the disregulated expression of *Snap25* and *Snap23* by qRT-PCR (Fig 4F).

The network analysis showed that DYRK1A controls 42,3 % of the network nodes and 69,4 % of the network seeds, (DEGs known to be involved in brain synaptic pathways) via 2nd level interactors. Hence, DYRK1A could control the DS synaptic network via PPI and regulatory interactions. Furthermore, the biological cascades centred on GSK3B, DYRK1A and RHOA are highly interconnected (S15 fig) and in fact several interactors of RHOA are connected and could somehow modulate a higher percentage (75 and 68.5%) of the nodes of the network and synaptic seeds. Interestingly, *RhoA* was not found altered in the differential expression analysis, instead it was a node introduced in the network to have a fully connected synaptic PPI network. We checked whether the RHOA pathway was altered in the Dp1Yey (Fig 4A). We found no changes in the expression of RHOA, confirming the transcriptomics analyses, but a significant decrease of the phosphorylation of the c (P-MLC) in the Dp1Yey hippocampi compared to control. Thus, the RHOA pathways appeared to be down-regulated in the Dp1Yey DS mouse models.

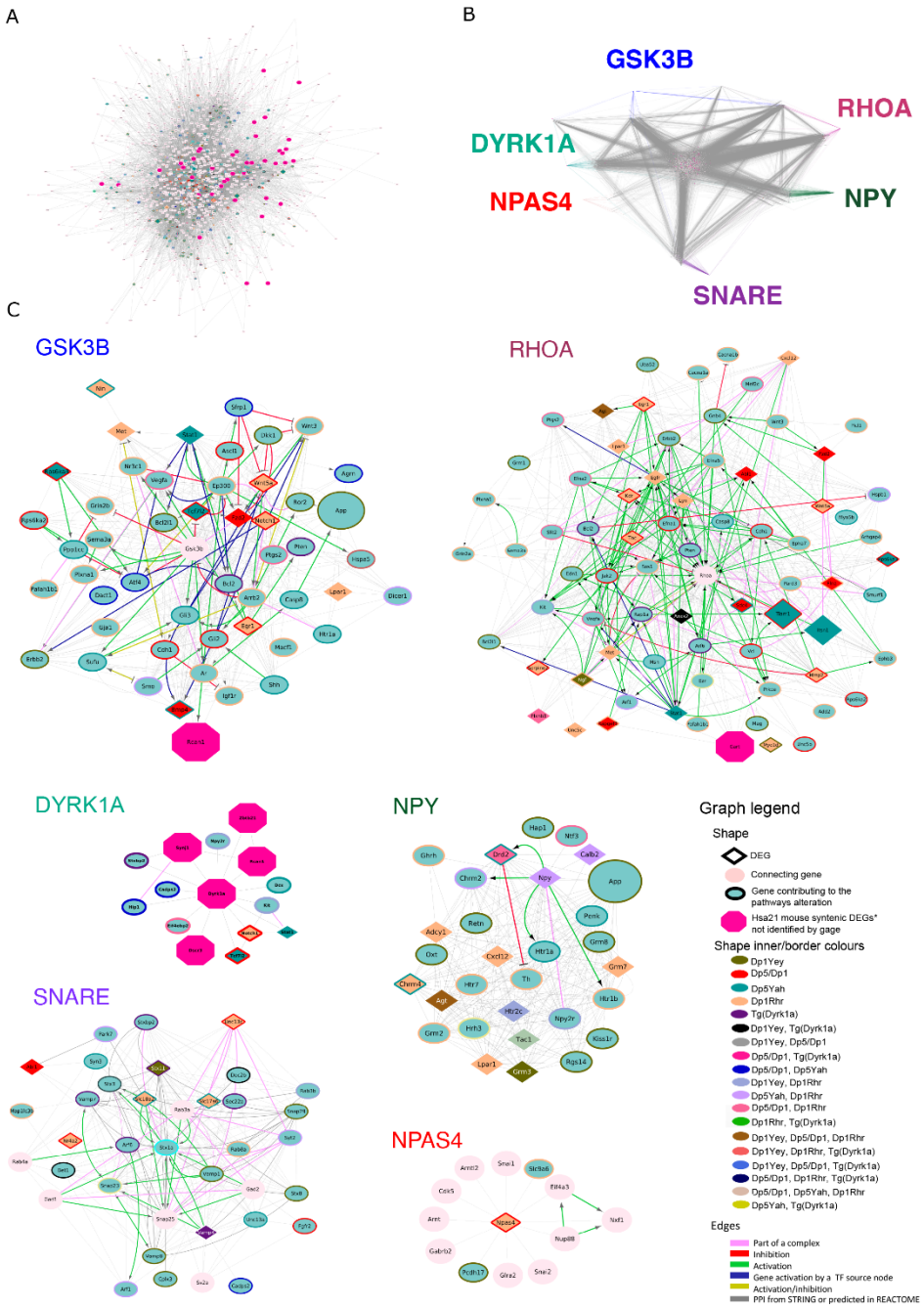

Figure 3: Protein-protein interaction networks involving DEGs linked to the synaptic function. (A) STRING04 MinPPINet of genes involved in synaptic function visualized using the edge weighed spring embedded layout by betwenness index in Cytoscape. The network was built by querying STRING and selecting the PPIs with a medium confidence score (CS=0.4) coming from all sources of evidence. The shapes of the nodes represent the following information: Shapes: i)Pallid pink ellipses: represent connecting proteins added to assure the full connectivity of the network; ii) pink octagons, represent HSA21 syntenic genes in mouse not identified as contributing to the meta-pathway dysregulation by GAGE; iii) green inner coloured ellipses, genes identified by GAGE after q-val <0.1 cut off to be contributing even slightly, to any pathway of those found dysregulated inside the meta-pathway. If the size is similar to the octagons, they are also HSA21 syntenic genes in mouse. Additionally, the border colour represents the mouse model multi group where those genes are found altered in; iv) diamonds, genes identified by GAGE after q-val <0.1 cut off and also by FCROS as DEGs.

(B) Network Structure Decomposition of the STRING04 MinPPINet. Highlighting in different colors the interactions of GSK3B, NPY, SNARE proteins, DYRK1A and RHOA respectively. In the case of NPAS4, the interactions coloured correspond up to the first level interactions. (C) The six RegPPINets were extracted from the selection of each fo the following proteins and their 2nd interactors from STRING04 MinPPINet: RHOA, DYRK1A, GSK3B, NPY, SNARE proteins and NPAS4. Then, those were further annotated with regulatory information using REACTOME (See Supplementary information). The shapes of the nodes represent the following information: Shapes: i)Pallid pink ellipses: represent connecting proteins added to assure the full connectivity of the network; ii) pink octagons, represent HSA21 syntenic genes in mouse not identified as contributing to the meta-pathway dysregulation by GAGE; iii) green inner coloured ellipses, genes identified by GAGE after q-val <0.1 cut off to be contributing even slightly, to any pathway of those found dysregulated inside the meta-pathway. If the size is similar to the octagons, they are also HSA21 syntenic genes in mouse. Additionally, the border colour represents the mouse model multi group where those genes are found altered in; iv) diamonds, genes identified by GAGE after q-val <0.1 cut off and also by FCROS as DEGs. The edges colored represent the type of interaction annotated by following the PathPPI classification (Tang *et al.* 2015),and ReactomeFIViz annotations as follows i) The GErel edges indicating expression were colored in blue and repression in yellow. ii) PPrel edges indicating activation were coloured in green, inhibition in red. Iii) Interactions between proteins known to be part of complexes in violet. Iv) Predicted interactions were represented in grey including the PPI interactions identified by STRING DB (Szklarczyk *et al.* 2017) after merging both networks.

Npas4 pathway is up-regulated as a consequence of *Dyrk1a* overexpression

In our transcriptomics and network analysis, we found that *Npas4* was down-regulated in Tg(*Dyrk1a*), Dp1Rhr and Ts65Dn models and this gene level of expression is highly variable in the models (S11 Fig). *Npas4* belongs to the class of immediate early genes with *Arc*, *Fosb* and *Fos*. Light deprivation and then exposure is known to drive robust gene expression, with shared early-response genes and distinct sets of late-response genes in excitatory and inhibitory (E/I) neurons (73). *Npas4* was recently identified as a key in E/I balance in the visual cortex after light deprivation (74).

To confirm the impact of *Npas4* down regulation in Tg(*Dyrk1a*) mice, we performed qRT-PCR experiments to determine the specific early and late response genes altered in the visual cortex after light deprivation at 3 time points (1, 3 and 7.5 hours) after de novo light exposure (Fig 4B). The results showed that *Npas4* was clearly induced after light deprivation following 1 hour of light stimulation. Expression data revealed also a strong overexpression of *Npas4* following 1 hour of light stimulation in Tg(*Dyrk1a*) mice (Fig 4C). On the contrary, the expression of late

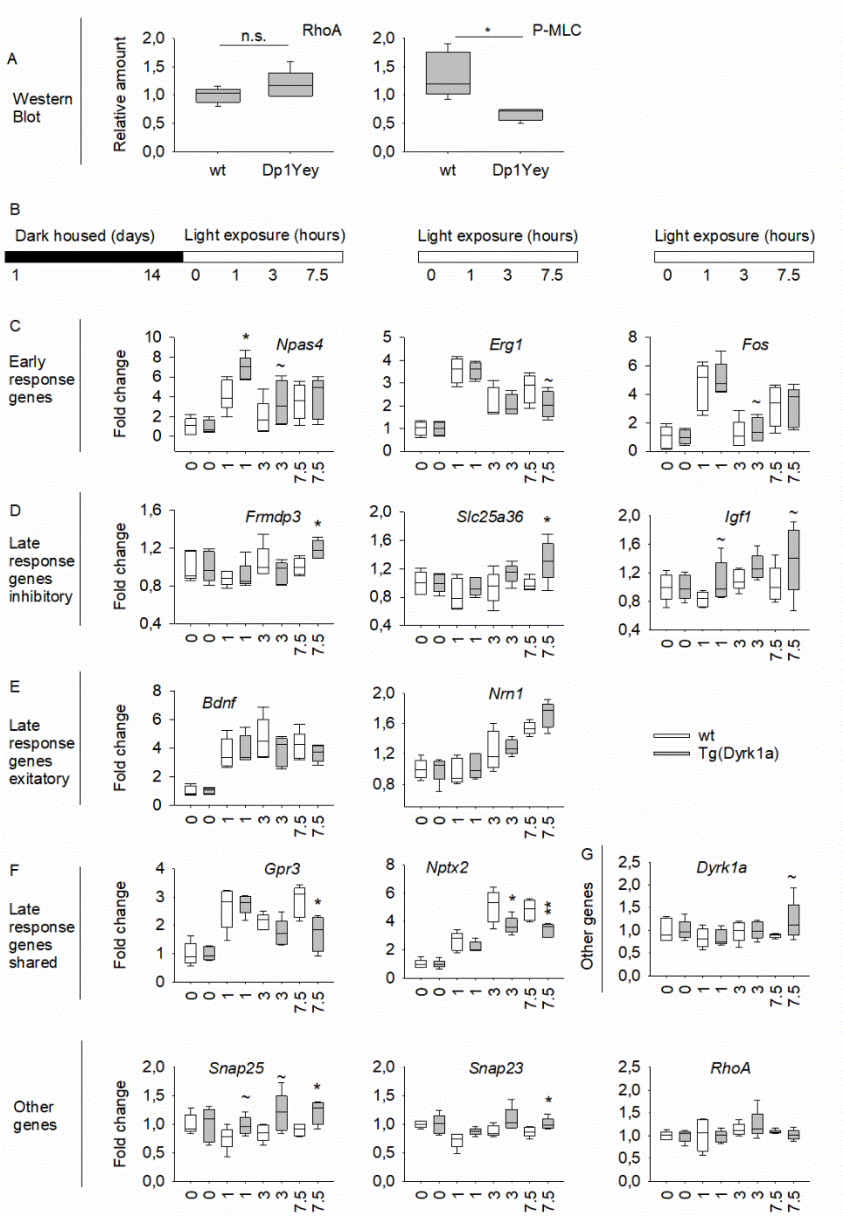

Figure 4: Evaluating Npas4 and RhoA pathways in DS models (A) RHOA pathway was altered in the Dp1Yey. Western blot analysis was revealed no changes in the expression of RHOA but a significant decrease of the phosphorylation of the Myosin light chain (P-MLC) in the Dp1Yey hippocampi compared to control. (B) Mice were housed in total darkness for 14 days and then were subsequently exposed to light for 0, 1, 3 or 7.5 h. Relative expression levels were determined, and fold change were calculated for each condition. Genotypes differences in fold change were assessed by T Test. (C) Only the fold change for early response genes *Npas4* was up-regulated in Tg(*Dyrk1a*) mice compared to wt at 1 hours of light induction. (D) The late responses genes specific to inhibitory neurons *Frmdp3*, *Slc25a36* and *Igf1* were up-regulated after 7.5 hours of light induction. (E) The fold change of late responses genes specific to excitatory neurons *Bdnf* and *Nrn1* were unchanged. (F) The fold change of late response genes shared by excitatory and inhibitory neurons *Gpr3* and *Nptx2* were downregulated after 3 and/or 7.5 hours of light induction. (G) *Dyrk1a* and *RhoA* showed a similar fold change along the different condition whereas *Snap25* and *Snap23* presented an increased enrichment for the 7.5 hours condition. Data are presented as box plots with the median and quartiles.

response genes specific for inhibitory neurons (*Frmdp3, Slc25a36* and *Igf1,* Fig 4D) and late response genes (*Grp3* and *Nptx2,* Fig 4F*)* were altered after 7.5 hours of light stimulation in Tg(*Dyrk1a*). Interestingly, late response genes specific to exitatory neurons (*Bdnf* and *Nrn1,* Fig 4E) were not affected. The *Snap25, Snap23* candidate genes found in our analysis showed an altered expression after 7.5hours of light stimulation while *Dyrk1a* and *RhoA* levels were not affected (Fig 4F). These results indicate that inhibitory pathways controlled by *Npas4* were affected by *Dyrk1a* overexpression. Furthermore, the network analyses highlighted NPAS4 as a potential modulator of the synaptic dysfunction as via well connected interactors, NPAS4 could affect the main altered biological cascades plus the GABA and NMDA receptors involved in the modulation of the excitatory / inhibitory balance of the brain (73).

Discussion

In this study, we explored the in vivo DS mouse model library focusing on the region homologous to Hsa21 found on Mmu16, to decode the DS genotype-phenotype relationships and further underlie genetic interactions between different regions. For this, we assessed 6 partial DS trisomic models, a transgenic model overexpressing one copy of *Dyrk1a*, plus some additional combination of models, using a standardized behavioural pipeline focused on hippocampus-dependent memory processes.

In this unique parallel comparison, we found that the spontaneus alternation in Y-maze, was altered in most of the models (except the Dp5Yah alone; Fig 5). The minimal common genetic part of these lines was the overexpression of *Dyrk1a* and the result observed for the transgenic Tg(*Dyrk1a*). Altogether, our results previously obtained, support DYRK1A as a main driver of this DS cognitive phenotype (25). wSimilarly, DYRK1A overdosage is a major cause for the increased exploration in the open field in Ts65Dn, Dp5/Tg(*Dyrk1a*) and Tg(*Dyrk1a*), but not in other models. While the Dp1Rhr Ds model was not affected, one can hypothesized that another loci intefere with *Dyrk1a* overdosage in this model. The situation

should be even more complex with more additional genetic interaction. No phenotype is observed for the distance travelled in the Dp1Yey, Dp5/Dp1, Dp5 or Dp1 models while the Ts65Dn, the Dp5-Tg(Dyrk1a) and the Tg(Dyrk1a) models showed an increase in this variable. Thus the overexpression of Dyrk1a is able on its own, or combined with Dp5Yah, to induce the increase in distance travelled while some loci which are not trisomic only in the Dp5/Dp1 model are able to suppress this effect, that can be reinduced by other trisomic loci specific to the Ts65Dn (see below). Altogether our results suggest that many different genetic influence (at least 3 for the distance travelles acts on different behavioural variables in DS models

Similar analysis of the novel object reognition test with 2 ditinct retention time highlight several loci. Indeed the phenotype of novel object recognition test, with 1h of retention time, only pointed to Dyrk1a overexpression, with at least one suppressing loci in the Dp1Rhr trisomic region. The novel object recognition with 24h of retention unravelled deficiency in most of the models, except in the Dp5Yah and Dp5/Dp1, suggesting that there are at least two causative loci: one located in the Dp3Yah region and *Dyrk1a*; and presumably two modifier interacting loci: one located in the Dp5Yah and another in the Dp1Rhr regions (Fig 5). Altogether our results suggested that depending on the variable observed in the behavioural test, many genetic interaction takes place to build the behavioural phenotyping outcome in DS mouse models with several loci, spread along the Mmu16, including *Dyrk1a*. Alltogether these locis interracted with different degrees of complexity to induce similar behavioural phenotype outcomes.

As expected, we found deficits in the Ts65Dn mice similar to the ones previously published in the Y-maze, the open field, NOR, MWM and contextual fear conditioning (52, 75) tests. Strinkingly, thigmotaxis and time in the target quadrant in the probe test of the MWM were two variables only modified in the Ts65Dn trisomic model while the Dp1Yey, that carry a duplication of the complete syntenic Mmu16 region, was less affected as described before (76, 77). Remarkably, the Dp5Yah mice, with a duplication from *Cyyr1* to *Clic6*, displayed no

664

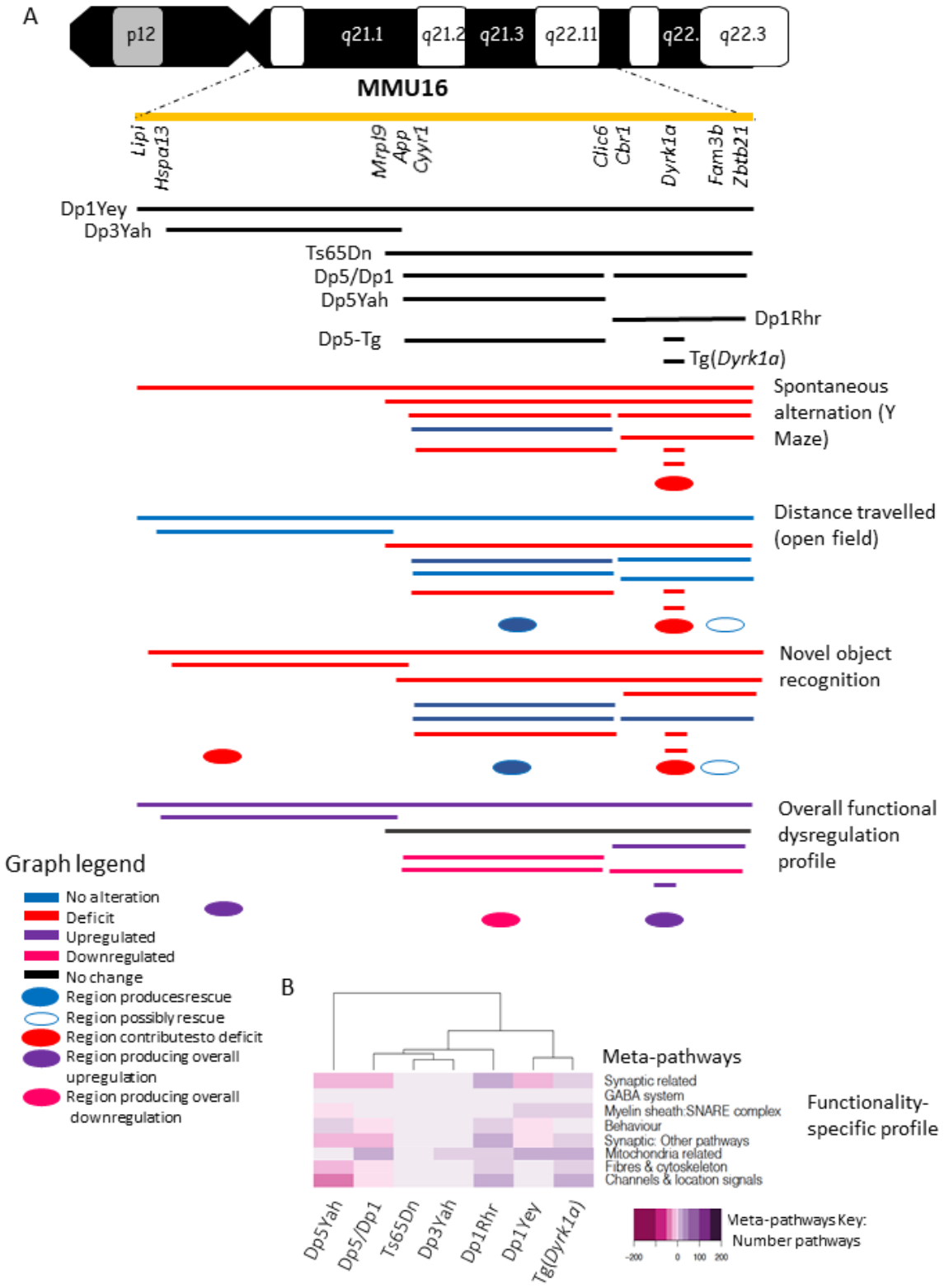

665

666 **Figure 5: Genotype correlation associated to behaviour phenotype in partial trisomic DS**
667 **model.** Here we highlight the duplicated region carried on each model with the corresponding
668 syntenic region in the human chromosome 21 together with the main behavioral and
669 transcriptomics results pointing to the existence of region specific phenotypes and functional

alteractions. The black lines represents the duplicated syntenic regions to human chromosome 21 on each model (represented in the yellow line). The blue lines represents the behavioral results where no alteration was found, instead the red lines identifed the tests with deficits. Over the transcriptomics meta-pathways fucntional profile summary picture, in purple is highlighted upregulation whereas in pink downregulation. The intensity of the color stands for the number of pathways included on each meta-pathway from the total number of pathways found altered on each model.

deficits on its own in all the tests done and showed the lower number of DEGs in the hippocampi. This might indicate that the *Cyrr1-Clic6* region was not sufficient to induce by itself cognitive defects. However, this syntenic region includes the genes *Sod1*, *Olig1*, *Olig2,* *Rcan1* and *Synj1*, proposed before as inducing early DS cognitive phenotype (78-81). Nevertheless, no defects were found in the Dp5/Dp1 mice contrary to the Ts65Dn in the open field or less severe in the NOR test (see below). This indicates the existence of a key modulator in the *Cyyr1-Clic6* region. The major behavioural alterations found in the Ts65Dn should result from the influence of different factors: first the genes homologous to Hsa21; then the presence of the freely segregating mini-chromosome (82), and also the trisomy of about 60 Mmu17 centromeric genes, non homologous to Hsa21(16), and overexpressed in the hippocampus of Ts65Dn mice. Especially the overdosage of *Tiam2* and *Synj2,* located on the Mmu17 centromeric region, could exacerbate the effect of the overexpression of their respecitve paralogs *Tiam1* and *Synj1* (81, 83). Strikingly, transcriptomic analysis showed a different global disruption of the genome expression in the Ts65Dn hippocampi, compared to the other trisomic models with segmental duplications. This is emphasized by the low correlation of DEGs and deregulated pathways between Ts65Dn, Dp1Yey and Dp5/Dp1. Overall, we can hypothesize that there is a suppression effect in the Dp1Yey model compared to the Ts65Dn induced phenotypes, due either to genes overexpressed and located upstream of *Mrpl39*, or to genes located on the non-homologous region in the Ts65Dn minichromosome, or to the freely segregating minichromsome.

Similar to cognition, brain morphology was affected differently in some DS models. For example, the Dp1Rhr rather showed an increase of size in many brain region compared to the

other DS models, where a decrease of size is observed like in Dp1Yey, Ts65Dn and Tg(*Dyrk1a*). Changes were found in several regions including the basal forebrain septum, a predominant source of cortical cholinergic input with an early substantial loss of basal forebrain cholinergic neurons (BFCN); as a constant feature of Alzheimer's disease and other deficits in spatial learning and memory (84). Individuals with DS exhibit progressive degeneration of BFCN (85). Similarly, significant loss of BFCN is present in the Ts65Dn (for review see (86)) and moreover, our results seem to indicate a default in BFCN in Dp1Yey and Tg(*Dyrk1a*) too. Several findings suggest that overexpression of amyloid protein precursor (APP) play a major role and could be strictly necessary for BFCN cell loss (87), thus, future investigation in Tg(*Dyrk1a*) should reveal if BFCN loss is present even without APP overexpression. Besides, only the Ts65Dn present an enlargement on the ventricles, which was previously associated with a decrease of cortical neurogenesis in the brains of Ts1Cje and Ts2Cje mouse models (33).

The comparative genome wide expression profiling in the mouse hippocampus revealed that not a single gene or a single region can recapitulate the whole disregulation. The overall effect results from a complex interplay of a few trisomic overexpressed genes and other genes spread along the genome, shown by the majority of DEGs not being Hsa21 genes (S3 table). Additionally, we identified 34 trisomic DEGs (TEGs) with regulatory activity (Transcription factors, chromatin modellers...) as *Mir99a*, *Usp16*, *Erg* or *Rcan1* that may be involved in the models' changed regulatory landscape. Indeed, *RCAN1* and *USP16* were found upregulated in all human brain datasets (cerebrum and cerebellum) and USP16 was also found as DEG upregulated in heart and adult fibroblasts while MIR99A was found upregulated in adult fibroblast (62). Nevertheless, the DEGs expression was strongly correlated and conserved in Mmu16 based DS models. This is similar to the behavioural results obtained where related phenotypes were found in models carrying correlated partial duplications. Unexpectedly, Dp1Yey DEGs correlation is closer to Tg(*Dyrk1a*) than to Ts65Dn (42% against 25%) and there is a negative correlation between Dp3Yah & Dp5Yah (22%) and Tg(*Dyrk1a*) & Dp5Yah

(13%) pointing out to a different gene dysregulation on these models and to the existence of epistasis with some regulatory trisomic genes countering the effect of genes in other trisomic regions. Carrying an in depth functional annotation analysis, we could not find a unique common pathway altered in all models. Nevertheless, due to the high redundancy in both GO and KEGG terms and the genes associated with each term, grouping the pathways shared at least by two models (materials & methods) in 8 functional groups unravelled 8 major meta-pathways with ribosome and mitochondrial function, transcription & epigenomics regulation, and the synapse function categories highly affected. We also found a strong upregulation of genes involved in the InterferonB pathway (S13 FigB) as some interferon receptors are found upregulated in Mmu16 DS models. As such *Ifnar2* and *Il10rb* were found upregulated in all the mice lines (except Tg(*Dyrk1a*)) pointing to a potentially critical role in the interferon pathway dysregulation. The same was observed with other genes as *Irgn1,Ifit1, Ifit2* or *Ndufa13*. This upregulation of the interferonB pathways was previously reported in the Ts1Cje mouse model (88, 89) and linked to a possible increase of activity of the Jak-Stat signaling pathway as recorded here by the up regulation of *Stat1*.

Expression of genes involved in long-term synaptic potentiation (LTP) and synaptic plasticity were decreased in Dp1Yey, Dp5Yah, Dp1Rhr, Dp5/Dp1 models respectively, corroborating previous reports in different DS mouse models and in vitro studies. The only upregulated pathways were the myelin sheath and SNARE; both found in Dp1Yey and Tg(Dyrk1A) models. Interestingly, models carrying the Dp1Rhr region duplication showed a dysregulation mainly in synapse transmission, plasticity and LTP, while models carrying the Dp5Yah region duplication showed a dysregulation associated with genes involved in stemness and differentiation. Together, the models with both Dp5Yah & Dp1Rhr duplicated regions, were involved in post-synapse modulation and transmission. Moreover, there is a high number of shared DEGs between these pathways and the models giving rise to a high intermodel inter-pathway connectivity with genes strongly connected into major subnetwork biological cascades

752 centralized over 6 different cascades controlled by DYRK1A, GSK3B, NPY, SNARE complex,
753 RHOA and NPAS4 that play a crucial role in the brain function. DYRK1A is a well recognized
754 driver of DS phenotypes and the target of several therapeutic approaches (25, 51). DYRK1A
755 was also shown to have interaction with GSK3B and NPY in DS models (25, 90-94). SNARE
756 complex protein were affected and it is interesting to see that they were also found modified in
757 a DS model for the region homologous to Hsa21 on Mmu17 (71). RHOA is a member of the
758 RHO GTPase involved in several intellectual disabilities that affects dendritic structure in adult
759 neurons (95-98), a phenotype also described in some DS models (99-101) or linked to
760 DYRK1A (102, 103).

761 Organizing the network to follow the betweenness centrality index values, RHOA,
762 DYRK1A, GSK3B, and their interactors were more closely knitted together and populated the
763 central part of the network while SNARE, NPAS4 and NPY with their first- and second-layer
764 interactors were more in the periphery of the network. This strong interconnectivity has a
765 double interesting effect: it makes the full network really sensible to targeted attack against
766 these proteins and, at the same time, the network would be robust against the attacks if the
767 attack does not target several proteins simultaneously; for example during a drug trial. Thus,
768 studying further closely connected altered genes and understanding the interactions could
769 provide novel insights into the possible molecular mechanism explaining why so many
770 compounds, including DYRK1A specific kinase inhibitors, can restore learning and memory in
771 DS models (51, 104-106). Additionally, these nodes show a high number of connections.
772 Indeed, organising the network using the betweenness index, these nodes and their interactors
773 occupy the centre of the network showing the extreme importance of these nodes for the
774 stability of the network in terms of network theory. Moreover, similar to the observation in DS
775 patients, where the affectation/severity of the gene dysfunction vary for one patient, we
776 proposed here that different DS mouse models show different signalling cascades that were
777 affected with several members strongly interconnected and affecting brain dysfunction leading

778 to similar behavioural phenotypes; may be one possible explanation of the developmental
779 instability hypothesis, which postulates that the non specific triplication of a relative small
780 number of genes causes genetic imbalance with wide impact on global gene expression. This
781 hypothesis should be taken into account when therapeutic assay are planned. The result in one
782 partial trisomic mouse model should be replicated in more genetically complex models to test
783 potential genetic influencial factor (43, 51, 71). This is probably the limit of the model, even if
784 the mechanisms of behaviour and memory are common between mice and human, the
785 complexity of the system is lower. Conducting the same studies in more complex animal
786 models, carrying all the trisomic genes homologous to Has21, probably would definetely permit
787 a better deciphering of genes impacting on cognitive behaviour.
788

789 ## Conclusion

790 Taking advantage of DS mouse models, we investigated behavior and cognition, brain
791 morphology and hippocampal gene expression in a standard and controlled way. We unraveled
792 how multiple genetic interactions between different regions of the chromosome 21 contribute
793 in altering the outcome of the behavioural, morphological and molecular/pathways phenotypes.
794 Nonetheless we found that overlapping DS models show convergence in the biological
795 cascades altered, observed via building protein-protein interaction and regulatory networks,
796 and centred on 6 main hubs: DYRK1A, GSK3β, NPY, SNARE, RHOA and NPAS4. Four of
797 them were already described to be altered in some DS models, and we validated two additional
798 ones, RHOA and NPAS4. As such we have built a novel vision of the existing altered gene-
799 gene crosstalk and molecular mechanisms, with 6 specific highly interconnected hubs in DS
800 models, that should become central to advance in our understanding of DS neurobiology and
801 therapy development.
802

803 ## Acknowledgements

We would like to thank members of the research group, of the IGBMC laboratory and of the ICS. We are grateful to the IGBMC microarray and Sequencing platform and particularly C. Thibault-Carpentier, for providing us access to microarray. We extend our thanks to the animal care-takers of the ICS who are in charge of the mice wellness. We also thank F.Riet, C. Mittelhaeuser, A. Lux and V. Alunni and D. Dembele for expert technical assistance and useful discussion.We would like to aknowledge that Maria del Mar Muñiz Moreno was an IGBMC International PhD Programme fellow supported by LabEx INRT funds (ANR-10-LABX-0030-INRT).

Competing interests

The authors have no competing interest. This work has been supported by the National Centre for Scientific Research (CNRS), the French National Institute of Health and Medical Research (INSERM), the University of Strasbourg (Unistra), the French state funds through the “Agence Nationale de la Recherche” under the frame programme Investissements d’Avenir labelled ANR-10-IDEX-0002-02, ANR-10-LABX-0030-INRT, ANR-10-INBS-07 PHENOMIN to YH. The funders had no role in study design, data collection and analysis, decision to publish, or preparation of the manuscript.

References

1. Lejeune J, Turpin R, Gautier M. [Mongolism; a chromosomal disease (trisomy).]. Bull Acad Natl Med. 1959;143(11-12):256-65.
2. Antonarakis SE, Lyle R, Dermitzakis ET, Reymond A, Deutsch S. Chromosome 21 and down syndrome: from genomics to pathophysiology. Nat Rev Genet. 2004;5(10):725-38.
3. Oliver TR, Feingold E, Yu K, Cheung V, Tinker S, Yadav-Shah M, et al. New insights into human nondisjunction of chromosome 21 in oocytes. PLoS Genet. 2008;4(3):e1000033.
4. McCormick MK, Schinzel A, Petersen MB, Stetten G, Driscoll DJ, Cantu ES, et al. Molecular genetic appoach to the characterization of the "Down syndrome region" of chromosome 21. Genomics. 1989;5(2):325-31.
5. Korbel JO, Tirosh-Wagner T, Urban AE, Chen XN, Kasowski M, Dai L, et al. The genetic architecture of Down syndrome phenotypes revealed by high-resolution analysis of human segmental trisomies. Proceedings of the National Academy of Sciences of the United States of America. 2009;106(29):12031-6.
6. Korenberg JR. Molecular mapping of the Down syndrome phenotype. Prog Clin Biol Res. 1990;360:105-15.
7. Lyle R, Béna F, Gagos S, Gehrig C, Lopez G, Schinzel A, et al. Genotype-phenotype correlations in Down syndrome identified by array CGH in 30 cases of partial trisomy and partial monosomy chromosome 21. Eur J Hum Genet. 2009;17(4):454-66.
8. Delabar JM, Theophile D, Rahmani Z, Chettouh Z, Blouin JL, Prieur M, et al. Molecular mapping of twenty-four features of Down syndrome on chromosome 21. Eur J Hum Genet. 1993;1(2):114-24.
9. Korenberg JR, Chen XN, Schipper R, Sun Z, Gonsky R, Gerwehr S, et al. Down syndrome phenotypes: the consequences of chromosomal imbalance. Proc Natl Acad Sci U S A. 1994;91(11):4997-5001.
10. Rahmani Z, Blouin JL, Creau-Goldberg N, Watkins PC, Mattei JF, Poissonnier M, et al. Critical role of the D21S55 region on chromosome 21 in the pathogenesis of Down syndrome. Proc Natl Acad Sci U S A. 1989;86(15):5958-62.
11. Herault Y, Delabar JM, Fisher EMC, Tybulewicz VLJ, Yu E, Brault V. Rodent models in Down syndrome research: impact and future opportunities. Disease Models & Mechanisms. 2017;10(10):1165-86.
12. Gupta M, Dhanasekaran AR, Gardiner KJ. Mouse models of Down syndrome: gene content and consequences. Mammalian Genome. 2016;27(11-12):538-55.
13. Muñiz Moreno MDM, Brault V, Birling MC, Pavlovic G, Herault Y. Modeling Down syndrome in animals from the early stage to the 4.0 models and next. Prog Brain Res. 2020;251:91-143.
14. Herault Y, Duchon A, Velot E, Marechal D, Brault V, Dierssen M, et al. The in vivo Down syndrome genomic library in mouse. Down Syndrome: From Understanding the Neurobiology To Therapy. 2012;197:169-97.
15. Reeves RH, Irving NG, Moran TH, Wohn A, Kitt C, Sisodia SS, et al. A MOUSE MODEL FOR DOWN-SYNDROME EXHIBITS LEARNING AND BEHAVIOR DEFICITS. Nature Genetics. 1995;11(2):177-84.
16. Duchon A, Raveau M, Chevalier C, Nalesso V, Sharp AJ, Herault Y. Identification of the translocation breakpoints in the Ts65Dn and Ts1Cje mouse lines: relevance for modeling down syndrome. Mammalian Genome. 2011;22(11-12):674-84.
17. Reinholdt LG, Ding YM, Gilbert GT, Czechanski A, Solzak JP, Roper RJ, et al. Molecular characterization of the translocation breakpoints in the Down syndrome mouse model Ts65Dn. Mammalian Genome. 2011;22(11-12):685-91.

18. Davisson MT, Schmidt C, Reeves RH, Irving NG, Akeson EC, Harris BS, et al. Segmental trisomy as a mouse model for Down syndrome. Prog Clin Biol Res. 1993;384:117-33.
19. Li Z, Yu T, Morishima M, Pao A, LaDuca J, Conroy J, et al. Duplication of the entire 22.9 Mb human chromosome 21 syntenic region on mouse chromosome 16 causes cardiovascular and gastrointestinal abnormalities. Hum Mol Genet. 2007;16(11):1359-66.
20. Olson LE, Richtsmeier JT, Leszl J, Reeves RH. A chromosome 21 critical region does not cause specific Down syndrome phenotypes. Science. 2004;306(5696):687-90.
21. Olson LE, Roper RJ, Baxter LL, Carlson EJ, Epstein CJ, Reeves RH. Down syndrome mouse models Ts65Dn, Ts1Cje, and Ms1Cje/Ts65Dn exhibit variable severity of cerebellar phenotypes. Dev Dyn. 2004;230(3):581-9.
22. Olson LE, Roper RJ, Sengstaken CL, Peterson EA, Aquino V, Galdzicki Z, et al. Trisomy for the Down syndrome 'critical region' is necessary but not sufficient for brain phenotypes of trisomic mice. Hum Mol Genet. 2007;16(7):774-82.
23. Belichenko NP, Belichenko PV, Kleschevnikov AM, Salehi A, Reeves RH, Mobley WC. The "Down syndrome critical region" is sufficient in the mouse model to confer behavioral, neurophysiological, and synaptic phenotypes characteristic of Down syndrome. J Neurosci. 2009;29(18):5938-48.
24. Guedj F, Pereira PL, Najas S, Barallobre MJ, Chabert C, Souchet B, et al. DYRK1A: a master regulatory protein controlling brain growth. Neurobiol Dis. 2012;46(1):190-203.
25. Duchon A, Herault Y. DYRK1A, a Dosage-Sensitive Gene Involved in Neurodevelopmental Disorders, Is a Target for Drug Development in Down Syndrome. Frontiers in Behavioral Neuroscience. 2016;10.
26. De la Torre R, De Sola S, Pons M, Duchon A, Martinez de Lagran M, Farre M, et al. Epigallocatechin-3-gallate, a DYRK1A inhibitor, rescues cognitive deficits in Down syndrome mouse models and in humans. Molecular Nutrition & Food Research. 2014;58(2):278-88.
27. Altafaj X, Martin ED, Ortiz-Abalia J, Valderrama A, Lao-Peregrin C, Dierssen M, et al. Normalization of Dyrk1A expression by AAV2/1-shDyrk1A attenuates hippocampal-dependent defects in the Ts65Dn mouse model of Down syndrome. Neurobiology of Disease. 2013;52:117-27.
28. Garcia-Cerro S, Martinez P, Vidal V, Corrales A, Florez J, Vidal R, et al. Overexpression of Dyrk1A Is Implicated in Several Cognitive, Electrophysiological and Neuromorphological Alterations Found in a Mouse Model of Down Syndrome. Plos One. 2014;9(9).
29. Pennington BF, Moon J, Edgin J, Stedron J, Nadel L. The neuropsychology of Down syndrome: evidence for hippocampal dysfunction. Child Dev. 2003;74(1):75-93.
30. Nadel L. Down's syndrome: a genetic disorder in biobehavioral perspective. Genes Brain Behav. 2003;2(3):156-66.
31. Brown SDM, Hancock JM, Gates H. Understanding mammalian genetic systems: The challenge of phenotyping in the mouse. Plos Genetics. 2006;2(8):1131-7.
32. Mandillo M, Tucci V, Holter SM, Meziane H, Al Banchaabouchi M, Kallnik M, et al. Reliability, robustness, and reproducibility in mouse behavioral phenotyping: a cross-laboratory study. (vol 34, pg 243, 2008). Physiological Genomics. 2010;40(3):217-.
33. Ishihara K, Amano K, Takaki E, Shimohata A, Sago H, Epstein CJ, et al. Enlarged Brain Ventricles and Impaired Neurogenesis in the Ts1Cje and Ts2Cje Mouse Models of Down Syndrome. Cerebral Cortex. 2010;20(5):1131-43.
34. Raveau M, Nakahari T, Asada S, Ishihara K, Amano K, Shimohata A, et al. Brain ventriculomegaly in Down syndrome mice is caused by Pcp4 dose-dependent cilia dysfunction. Human Molecular Genetics. 2017;26(5):923-31.

35. Guedj F, Pereira PL, Najas S, Barallobre MJ, Chabert C, Souchet B, et al. DYRK1A: A master regulatory protein controlling brain growth. Neurobiology of Disease. 2012;46(1):190-203.
36. Guedj F, Sebrie C, Rivals I, Ledru A, Paly E, Bizot JC, et al. Green Tea Polyphenols Rescue of Brain Defects Induced by Overexpression of DYRK1A. Plos One. 2009;4(2):8.
37. Brault V, Duchon A, Romestaing C, Sahun I, Pothion S, Karout M, et al. Opposite phenotypes of muscle strength and locomotor function in mouse models of partial trisomy and monosomy 21 for the proximal Hspa13-App region. PLoS Genet. 2015;11(3):e1005062.
38. Hoelter SM, Dalke C, Kallnik M, Becker L, Horsch M, Schrewe A, et al. "Sighted C3H" mice - a tool for analysing the influence of vision on mouse behaviour? Frontiers in Bioscience. 2008;13:5810-23.
39. Dubos A, Meziane H, Iacono G, Curie A, Riet F, Martin C, et al. A new mouse model of ARX dup24 recapitulates the patients' behavioural and fine motor alterations. Hum Mol Genet. 2018.
40. Arbogast T, Iacono G, Chevalier C, Afinowi NO, Houbaert X, van Eede MC, et al. Mouse models of 17q21.31 microdeletion and microduplication syndromes highlight the importance of Kansl1 for cognition. PLoS Genet. 2017;13(7):e1006886.
41. Ung DC, Iacono G, Méziane H, Blanchard E, Papon MA, Selten M, et al. Ptchd1 deficiency induces excitatory synaptic and cognitive dysfunctions in mouse. Mol Psychiatry. 2017.
42. Arbogast T, Ouagazzal AM, Chevalier C, Kopanitsa M, Afinowi N, Migliavacca E, et al. Reciprocal Effects on Neurocognitive and Metabolic Phenotypes in Mouse Models of 16p11.2 Deletion and Duplication Syndromes. PLoS Genet. 2016;12(2):e1005709.
43. Marechal D, Lopes Pereira P, Duchon A, Herault Y. Dosage of the Abcg1-U2af1 region modifies locomotor and cognitive deficits observed in the Tc1 mouse model of Down syndrome. PLoS One. 2015;10(2):e0115302.
44. Dembele D, Kastner P. Fold change rank ordering statistics: a new method for detecting differentially expressed genes. Bmc Bioinformatics. 2014;15.
45. Luo W, Friedman MS, Shedden K, Hankenson KD, Woolf PJ. GAGE: generally applicable gene set enrichment for pathway analysis. BMC Bioinformatics. 2009;10:161.
46. Ashburner M, Ball CA, Blake JA, Botstein D, Butler H, Cherry JM, et al. Gene ontology: tool for the unification of biology. The Gene Ontology Consortium. Nat Genet. 2000;25(1):25-9.
47. Esling P, Lejzerowicz F, Pawlowski J. Accurate multiplexing and filtering for high-throughput amplicon-sequencing. Nucleic Acids Res. 2015;43(5):2513-24.
48. Desai AP, Razeghin M, Meruvia-Pastor O, Pena-Castillo L. GeNET: a web application to explore and share Gene Co-expression Network Analysis data. PeerJ. 2017;5:e3678.
49. Vandesompele J, De Preter K, Pattyn F, Poppe B, Van Roy N, De Paepe A, et al. Accurate normalization of real-time quantitative RT-PCR data by geometric averaging of multiple internal control genes. Genome Biology. 2002;3(7).
50. Gardiner K, Fortna A, Bechtel L, Davisson MT. Mouse models of Down syndrome: how useful can they be? Comparison of the gene content of human chromosome 21 with orthologous mouse genomic regions. Gene. 2003;318:137-47.
51. Nguyen TL, Duchon A, Manousopoulou A, Loaëc N, Villiers B, Pani G, et al. Correction of cognitive deficits in mouse models of Down syndrome by a pharmacological inhibitor of DYRK1A. Dis Model Mech. 2018;11(9).
52. Faizi M, Bader PL, Tun C, Encarnacion A, Kleschevnikov A, Belichenko P, et al. Comprehensive behavioral phenotyping of Ts65Dn mouse model of Down Syndrome: Activation of pradrenergic receptor by xamoterol as a potential cognitive enhancer. Neurobiology of Disease. 2011;43(2):397-413.

53. Souchet B, Guedj F, Sahun I, Duchon A, Daubigney F, Badel A, et al. Excitation/inhibition balance and learning are modified by Dyrk1a gene dosage. Neurobiology of Disease. 2014;69:65-75.
54. Escorihuela RM, Fernández-Teruel A, Vallina IF, Baamonde C, Lumbreras MA, Dierssen M, et al. A behavioral assessment of Ts65Dn mice: a putative Down syndrome model. Neurosci Lett. 1995;199(2):143-6.
55. Martinez-Cue C, Baamonde C, Lumbreras M, Paz J, Davisson MT, Schmidt C, et al. Differential effects of environmental enrichment on behavior and learning of male and female Ts65Dn mice, a model for Down syndrome. Behavioural Brain Research. 2002;134(1-2):185-200.
56. Martinez-Cue C, Rueda N, Garcia E, Davisson MT, Schmidt C, Florez J. Behavioral, cognitive and biochemical responses to different environmental conditions in male Ts65Dn mice, a model of Down syndrome. Behavioural Brain Research. 2005;163(2):174-85.
57. Moran TH, Capone GT, Knipp S, Davisson MT, Reeves RH, Gearhart JD. The effects of piracetam on cognitive performance in a mouse model of Down's syndrome. Physiol Behav. 2002;77(2-3):403-9.
58. Rueda N, Florez J, Martinez-Cue C. Effects of chronic administration of SGS-111 during adulthood and during the pre- and post-natal periods on the cognitive deficits of Ts65Dn mice, a model of Down syndrome. Behavioural Brain Research. 2008;188(2):355-67.
59. Rueda N, Florez J, Martinez-Cue C. Chronic pentylenetetrazole but not donepezil treatment rescues spatial cognition in Ts65Dn mice, a model for Down syndrome. Neuroscience Letters. 2008;433(1):22-7.
60. Seo H, Isacson O. Abnormal APP, cholinergic and cognitive function in Ts65Dn Down's model mice. Exp Neurol. 2005;193(2):469-80.
61. Lockstone HE, Harris LW, Swatton JE, Wayland MT, Holland AJ, Bahn S. Gene expression profiling in the adult Down syndrome brain. Genomics. 2007;90(6):647-60.
62. Prandini P, Deutsch S, Lyle R, Gagnebin M, Vivier CD, Delorenzi M, et al. Natural gene-expression variation in Down syndrome modulates the outcome of gene-dosage imbalance. American Journal of Human Genetics. 2007;81(2):252-63.
63. Ait Yahya-Graison E, Aubert J, Dauphinot L, Rivals I, Prieur M, Golfier G, et al. Classification of human chromosome 21 gene-expression variations in Down syndrome: impact on disease phenotypes. American journal of human genetics. 2007;81(3):475-91.
64. Laffaire J, Rivals I, Dauphinot L, Pasteau F, Wehrle R, Larrat B, et al. Gene expression signature of cerebellar hypoplasia in a mouse model of Down syndrome during postnatal development. Bmc Genomics. 2009;10.
65. Sultan M, Piccini I, Balzereit D, Herwig R, Saran NG, Lehrach H, et al. Gene expression variation in 'Down syndrome' mice allows to prioritize candidate genes. Genome Biol. 2007;8(5):R91.
66. Mao R, Zielke CL, Zielke HR, Pevsner J. Global up-regulation of chromosome 21 gene expression in the developing Down syndrome brain. Genomics. 2003;81(5):457-67.
67. Olmos-Serrano JL, Kang HJ, Tyler WA, Silbereis JC, Cheng F, Zhu Y, et al. Down Syndrome Developmental Brain Transcriptome Reveals Defective Oligodendrocyte Differentiation and Myelination. Neuron. 2016;89(6):1208-22.
68. Guedj F, Pennings JL, Massingham LJ, Wick HC, Siegel AE, Tantravahi U, et al. An Integrated Human/Murine Transcriptome and Pathway Approach To Identify Prenatal Treatments For Down Syndrome. Sci Rep. 2016;6:32353.
69. Guedj F, Pennings JL, Wick HC, Bianchi DW. Analysis of adult cerebral cortex and hippocampus transcriptomes reveals unique molecular changes in the Ts1Cje mouse model of down syndrome. Brain Pathol. 2015;25(1):11-23.
70. Aziz NM, Guedj F, Pennings JLA, Olmos-Serrano JL, Siegel A, Haydar TF, et al. Lifespan analysis of brain development, gene expression and behavioral phenotypes in the

Ts1Cje, Ts65Dn and Dp(16)1/Yey mouse models of Down syndrome. Dis Model Mech. 2018;11(6).
71. Marechal D, Brault V, Leon A, Martin D, Pereira PL, Loaëc N, et al. Cbs overdosage is necessary and sufficient to induce cognitive phenotypes in mouse models of Down syndrome and interacts genetically with Dyrk1a. Hum Mol Genet. 2019.
72. Joazeiro CAP. Mechanisms and functions of ribosome-associated protein quality control. Nature Reviews Molecular Cell Biology. 2019;20(6):368-83.
73. Mardinly AR, Spiegel I, Patrizi A, Centofante E, Bazinet JE, Tzeng CP, et al. Sensory experience regulates cortical inhibition by inducing IGF1 in VIP neurons. Nature. 2016;531(7594):371-5.
74. Spiegel I, Mardinly AR, Gabel HW, Bazinet JE, Couch CH, Tzeng CP, et al. Npas4 Regulates Excitatory-Inhibitory Balance within Neural Circuits through Cell-Type-Specific Gene Programs. Cell. 2014;157(5):1216-29.
75. Smith GK, Kesner RP, Korenberg JR. Dentate Gyrus Mediates Cognitive Function in the Ts65Dn/DnJ Mouse Model of Down Syndrome. Hippocampus. 2014;24(3):354-62.
76. Belichenko PV, Kleschevnikov AM, Becker A, Wagner GE, Lysenko LV, Yu YE, et al. Down Syndrome Cognitive Phenotypes Modeled in Mice Trisomic for All HSA 21 Homologues. 2015(1932-6203 (Electronic)).
77. Yu T, Liu CH, Belichenko P, Clapcote SJ, Li SM, Pao AN, et al. Effects of individual segmental trisomies of human chromosome 21 syntenic regions on hippocampal long-term potentiation and cognitive behaviors in mice. Brain Research. 2010;1366:162-71.
78. Chakrabarti L, Best TK, Cramer NP, Carney RSE, Isaac JTR, Galdzicki Z, et al. Olig1 and Olig2 triplication causes developmental brain defects in Down syndrome. Nature Neuroscience. 2010;13(8):927-U39.
79. Xu R, Brawner AT, Li S, Liu JJ, Kim H, Xue H, et al. OLIG2 Drives Abnormal Neurodevelopmental Phenotypes in Human iPSC-Based Organoid and Chimeric Mouse Models of Down Syndrome. Cell Stem Cell. 2019;24(6):908-26 e8.
80. Ermak G, Cheadle C, Becker KG, Harris CD, Davies KJA. DSCR1 (Adapt78) modulates expression of SOD1. Faseb Journal. 2004;18(1):62-9.
81. Voronov SV, Frere SG, Giovedi S, Pollina EA, Borel C, Zhang H, et al. Synaptojanin 1-linked phosphoinositide dyshomeostasis and cognitive deficits in mouse models of Down's syndrome. Proceedings of the National Academy of Sciences of the United States of America. 2008;105(27):9415-20.
82. Antonarakis SE. Down syndrome and the complexity of genome dosage imbalance. Nat Rev Genet. 2016.
83. Chen C-K, Bregere C, Paluch J, Lu JF, Dickman DK, Chang KT. Activity-dependent facilitation of Synaptojanin and synaptic vesicle recycling by the Minibrain kinase. Nature Communications. 2014;5.
84. Dunnett SB, Everitt BJ, Robbins TW. THE BASAL FOREBRAIN CORTICAL CHOLINERGIC SYSTEM - INTERPRETING THE FUNCTIONAL CONSEQUENCES OF EXCITOTOXIC LESIONS. Trends in Neurosciences. 1991;14(11):494-501.
85. Isacson O, Seo H, Lin L, Albeck D, Granholm AC. Alzheimer's disease and Down's syndrome: roles of APP, trophic factors and ACh. Trends in Neurosciences. 2002;25(2):79-84.
86. Hamlett ED, Boger HA, Ledreux A, Kelley CM, Mufson EJ, Falangola MF, et al. Cognitive Impairment, Neuroimaging, and Alzheimer Neuropathology in Mouse Models of Down Syndrome. Current Alzheimer Research. 2015;13(1):35-52.
87. Salehi A, Delcroix JD, Belichenko PV, Zhan K, Wu CB, Valletta JS, et al. Increased App expression in a mouse model of Down's syndrome disrupts NGF transport and causes cholinergic neuron degeneration. Neuron. 2006;51(1):29-42.

88. Lee HC, Tan KL, Cheah PS, Ling KH. Potential Role of JAK-STAT Signaling Pathway in the Neurogenic-to-Gliogenic Shift in Down Syndrome Brain. Neural Plast. 2016;2016:7434191.
89. Ling KH, Hewitt CA, Tan KL, Cheah PS, Vidyadaran S, Lai MI, et al. Functional transcriptome analysis of the postnatal brain of the Ts1Cje mouse model for Down syndrome reveals global disruption of interferon-related molecular networks. BMC Genomics. 2014;15:624.
90. Woods YL, Cohen P, Becker W, Jakes R, Goedert M, Wang X, et al. The kinase DYRK phosphorylates protein-synthesis initiation factor eIF2Bepsilon at Ser539 and the microtubule-associated protein tau at Thr212: potential role for DYRK as a glycogen synthase kinase 3-priming kinase. Biochem J. 2001;355(Pt 3):609-15.
91. Hong SH, Lee KS, Kwak SJ, Kim AK, Bai H, Jung MS, et al. Minibrain/Dyrk1a regulates food intake through the Sir2-FOXO-sNPF/NPY pathway in Drosophila and mammals. PLoS Genet. 2012;8(8):e1002857.
92. Hernández-González S, Ballestín R, López-Hidalgo R, Gilabert-Juan J, Blasco-Ibáñez JM, Crespo C, et al. Altered distribution of hippocampal interneurons in the murine Down Syndrome model Ts65Dn. Neurochem Res. 2015;40(1):151-64.
93. Shukkur EA, Shimohata A, Akagi T, Yu WX, Yamaguchi M, Murayama M, et al. Mitochondrial dysfunction and tau hyperphosphorylation in Ts1Cje, a mouse model for Down syndrome. Human Molecular Genetics. 2006;15(18):2752-62.
94. King MK, Pardo M, Cheng YY, Downey K, Jope RS, Beurel E. Glycogen synthase kinase-3 inhibitors: Rescuers of cognitive impairments. Pharmacology & Therapeutics. 2014;141(1):1-12.
95. Khelfaoui M, Pavlowsky A, Powell AD, Valnegri P, Cheong KW, Blandin Y, et al. Inhibition of RhoA pathway rescues the endocytosis defects in Oligophrenin1 mouse model of mental retardation. Hum Mol Genet. 2009;18(14):2575-83.
96. da Silva JS, Dotti CG. Breaking the neuronal sphere: regulation of the actin cytoskeleton in neuritogenesis. Nat Rev Neurosci. 2002;3(9):694-704.
97. Ramakers GJA. Rho proteins, mental retardation and the cellular basis of cognition. Trends in Neurosciences. 2002;25(4):191-9.
98. Billuart P, Bienvenu T, Ronce N, des Portes V, Vinet MC, Zemni R, et al. Oligophrenin 1 encodes a rho-GAP protein involved in X-linked mental retardation. Pathol Biol (Paris). 1998;46(9):678.
99. Belichenko PV, Kleschevnikov AM, Salehi A, Epstein CJ, Mobley WC. Synaptic and cognitive abnormalities in mouse models of down syndrome: Exploring genotype-phenotype relationships. Journal of Comparative Neurology. 2007;504:329-45.
100. Belichenko PV, Masliah E, Kleschevnikov AM, Villar AJ, Epstein CJ, Salehi A, et al. Synaptic structural abnormalities in the Ts65Dn mouse model of Down Syndrome. J Comp Neurol. 2004;480(3):281-98.
101. Haas MA, Bell D, Slender A, Lana-Elola E, Watson-Scales S, Fisher EM, et al. Alterations to dendritic spine morphology, but not dendrite patterning, of cortical projection neurons in Tc1 and Ts1Rhr mouse models of Down syndrome. PLoS One. 2013;8(10):e78561.
102. Ori-McKenney KM, McKenney RJ, Huang HH, Li T, Meltzer S, Jan LY, et al. Phosphorylation of β-Tubulin by the Down Syndrome Kinase, Minibrain/DYRK1a, Regulates Microtubule Dynamics and Dendrite Morphogenesis. Neuron. 2016;90(3):551-63.
103. Thomazeau A, Lassalle O, Iafrati J, Souchet B, Guedj F, Janel N, et al. Prefrontal deficits in a murine model overexpressing the down syndrome candidate gene dyrk1a. J Neurosci. 2014;34(4):1138-47.
104. de la Torre R, de Sola S, Hernandez G, Farre M, Pujol J, Rodriguez J, et al. Safety and efficacy of cognitive training plus epigallocatechin-3-gallate in young adults with Down's

syndrome (TESDAD): a double-blind, randomised, placebo-controlled, phase 2 trial. Lancet Neurology. 2016;15(8):801-10.

105. Nakano-Kobayashi A, Awaya T, Kii I, Sumida Y, Okuno Y, Yoshida S, et al. Prenatal neurogenesis induction therapy normalizes brain structure and function in Down syndrome mice. Proc Natl Acad Sci U S A. 2017;114(38):10268-73.

106. Herault Y, Delabar JM, Fisher EMC, Tybulewicz VLJ, Yu E, Brault V. Rodent models in Down syndrome research: impact and future opportunities. Dis Model Mech. 2017;10(10):1165-86.

107. Revelle W. psych: Procedures for Psychological, Psychometric, and Personality Research. Northwestern University. 2019.

Supporting information

S1 Fig. Down syndrome mouse models analysed in the study. In the upper part of the plot the human chromosome 21 is represented, in yellow we highlighted the Hsa21 syntenic region found in mouse from *Lipi* to *Zbtb21* (known as *Zfp295* previously). The eight models analysed on this study Dp1Yey, Dp3Yah, Ts65Dn, Dp5/Dp1, Dp5Yah, Dp1Rhr, Tg(*Dyrk1a*), Dp5yah crossed with Tg(*Dyrk1a*) (noted as Dp5-Tg)) trisomic chomosomal regions were draw in comparison with the Hsa21 region.

S2 Fig. Quantile-Quantile plots to assess Normal distribution. The quantile-quantile plots (Q-Q plots) and Shapiro-Wilk test for the following behavioural datasets: Y-maze, NOR and OF were analysed to study how well our data could be modelled following a normal distribution. Only the distance travelled in OF did not reach the statistical significance level in the Shapiro-Wilk test.

S3 Figure. DS mouse models and Morris water maze. The MWM results are presented as distance travelled to reach the platform (A), speed (B) and % of distance travelled in the peripheral zone (C, Mean ± SEM). Ts65Dn mice were drastically impaired with an increase in distance travelled to reach the platform and in the distance travelled along the peripheral zone. Less drastically Tg(*Dyrk1a*) mice showed an increased distance travelled to escape the pool and in the peripheral zone (* $p<0.05$, ** $p<0.01$, *** $p<0.001$).

S4 Fig. DS mouse models and context and cue fear conditioning. The fear conditioning results are presented as inactivity periods in seconds (Mean±SEM). Only Ts56Dn mice present an impairment in context fear conditioning (* $p<0.05$, ** $p<0.01$, *** $p<0.001$).

S5 Fig. Comparison of the Z-score calculated from the MRI volume of different brain structures from the DS models. The structures affected in Tg(*Dyrk1a*) were also affected in Dp1Yey and Ts65Dn, whereas the Dp1Rhr mice.(Dp1Yey n=6wt and 6 Tg ; Ts65Dn n=5 wt and 6 Tg ; Tg(*Dyrk1a*) n=8 wt and 5 Tg ; Dp1Rhr n=7 wt and 7 Tg).

S6 Fig. Fold change expression levels of the genes analysed by the microarrays homologous to the Hsa21 mouse chromosome 16 (mm16). The genes are displayed following the order of their genomic start site coordinates. The duplicated areas for each mouse model appear shaded in the following colours, purple, grey, aquamarine, red, blue and golden for Dp1Yey, Dp3Yah, Ts65Dn, Dp1Rhr, Dp5Yah and Tg(*Dyrk1a*) respectively.

S7 Fig. Fold change expression levels of genes analyzed by the microarrays. (A) Fold change expression levels of the genes analysed by the microarrays part of the centromeric region of the mouse chromosome 17. The centromeric region of the mouse chromosome 17, is defined by the UCSC table browser as the region between the coordinates chr17:110000-3000000.The genes are displayed following the order of their start site genomic coordinates. The region duplicated in the Ts65Dn model non homologous to the hsa21, appears shaded in aquamarine. (B) Fold change expression levels of the genes homologous to the Hsa21 in mouse

chromosome 10 (mm10) and chromosome 17 (mm17) analysed by the microarrays. The genes are displayed following the order of their start site genomic coordinates.

S8 Fig. Number of deregulated probes per chromosomes per models. Trisomic mice have similar patterns with a pic of deregulated genes located on mouse chromosome 16. Tg Dyrk1a at contrary, present a global pattern of deregulated probes.

S9 Fig. Overview of the top 7 dysregulated genes (higher significance and fold change difference) for each mouse model over the global transformed expression profiles illustrated over volcano plots. The x axis and y axis represent the log2 fold change of the genes expression and the log transformed FDR values respectively. The genes whose fcros FDR value <0.05 are considered significant. These genes are represented in purple or pink and labelled as "Significant". Instead the genes whose abs (FC)> 1.4 are represented in green or pink and labelled "FC". Finally, the genes that don't comply these conditions are considered not significant.

S10 Fig. Gene expression correlation analyses. (A) Correlation of the 4328 differentially expressed genes (DEGs) expression levels on the different models. B) Correlation of the 75 differentially expressed trisomic genes (TEGs) expression levels on the different models. Each row represents a model pairwise correlation with the rest of the models. The density and histograms distribution of the gene expression values for each model is found in the medial diagonal (Black for DEGs, and pink for TEGs). The LOESS smoothed fit is represented by a red line. The plots were created in R using the pairs.panel function from Psych R CRAN package (107).

S11 Fig. Weighted networks representing the connectivity of the pathways included in the Cell structure & organelles, and the Transcription & epigenomic regulation meta-pathways. (A) Representation of the strength connecting the pathways included on the Cell Structure & organelle meta-pathway. (B) Representation of the strength connecting the pathways included on the Transcription & epigenomics regulation meta-pathway. The pathways incorporated in each meta-pathway were identified in the differential functional analysis (DFA) by GAGE after imposing a q-val <0.1 cut off. The connectivity between the pathways, (the edges weight or strength connecting the pathways) is represented by the number of altered genes identified by GAGE shared by each two pathways and is calculated based on the number of common genes within the pathways shared inter and intra mouse model (by each mouse model multi group defined) also grouped by regulation sense using the following formula* and represented by the thickness of the edges connecting the nodes (pathways) of the network. Each edges colour depends on the mouse models where those genes were identified (mouse model multi groups). Formula* = number of genes shared by each pathway on each model on each sense of regulation * factorRes with factorRes= 0.6.

S12 Fig. Weighted networks representing the connectivity of the pathways included in the Ribosome and Mitochondrial meta-pathways. (A) Representation of the strength connecting the pathways included on the Ribosome meta-pathway. (B) Representation of the strength connecting the pathways included on the Mitochondria meta-pathway. The pathways incorporated in each meta-pathway were identified in the differential functional analysis (DFA) by GAGE after imposing a q-val <0.1 cut off. The connectivity between the pathways, (the

edges weight or strength connecting the pathways) is represented by the number of altered genes identified by GAGE shared by each two pathways and is calculated based on the number of common genes within the pathways shared inter and intra mouse model (by each mouse model multi group defined) also grouped by regulation sense using the following formula* and represented by the thickness of the edges connecting the nodes (pathways) of the network. Each edges colour depends on the mouse models where those genes were identified (mouse model multi groups). Formula* = number of genes shared by each pathway on each model on each sense of regulation * factorRes with factorRes= 0.6

S13 Fig. Weighted network representing the connectivity of the pathways included in the Synaptic meta-group and the network representation of the genes linked to Interferon Beta (IFN-B) ungrouped pathway. (A) Representation of the strength connecting the pathways included on the Synaptic meta-pathway. The pathways incorporated in each meta-pathway were identified in the differential functional analysis (DFA) by GAGE after imposing a q-val <0.1 cut off. The connectivity between the pathways, (the edges weight or strength connecting the pathways) is represented by the number of altered genes identified by GAGE shared by each two pathways and is calculated based on the number of common genes within the pathways shared inter and intra mouse model (by each mouse model multi group defined) also grouped by regulation sense using the following formula* and represented by the thickness of the edges connecting the nodes (pathways) of the network. Each edges colour depends on the mouse models where those genes were identified (mouse model multi groups). Formula* = number of genes shared by each pathway on each model on each sense of regulation * factorRes, factorRes= 0.6. (B) Genes linked to Interferon Beta (IFN-B) ungrouped pathway, found altered in the different mouse model multi groups by GAGE. The genes are represented by the ellipse shapes instead the mouse model multi groups by lilac cuadrangles. If the genes were found up regulated then a red boder color was used around the ellipses. The genes also identified by FCROS as differentially expressed (DEG) were identified by a red colored inner ellipse.

S14 Fig. Protein-protein interaction and regulatory gene connectivity networks (RegPPINets) of genes involved in the synaptic meta-pathway highlighting biological cascades connectivity. The two sub-networks (A and B) were extracted from the STRING04 MinPPINet. This network was built querying STRING and selecting the PPIs with a medium confidence score (CS), CS=0.4 from all sources of evidence, and was further annotated with regulatory information using REACTOME (See Supplementary information). The shapes of the nodes represent the following information: Shapes: i)Pallid pink ellipses: represent connecting proteins added to assure the full connectivity of the network; ii) pink octagons, represent HSA21 syntenic genes in mouse not identified as contributing to the meta-pathway dysregulation by GAGE; iii) green inner coloured ellipses, genes identified by GAGE after q-val <0.1 cut off to be contributing even slightly, to any pathway of those found dysregulated inside the meta-pathway. If the size is similar to the octagons, they are also HSA21 syntenic genes in mouse. Additionally, the border colour represents the mouse model multi group where those genes are found altered in; iv) diamonds, genes identified by GAGE after q-val <0.1 cut off and also by FCROS as DEGs. (A) RegPPINet Sub-network extracted from the selection of RHOA 2nd interactors from STRING04 MinPPINet, highlighting RHOA 1st Interactors and DYRK1A and GSK3B interactors annotated with the regulatory information from REACTOME. (B) RegPPINet Sub-network extracted from the selection of NPAS4 2nd interactors from STRING04 MinPPINet. Inside of the ellipsoidal line shapes we highlighted NPAS4 interactors involved in the regulation of GABA receptors (cyan), of NMDA receptors (orange), SNARE complex (purple), RHOA (pink), GSK3B (Blue), both RHOA and GSK3B (black) and the genes linked to mitochondrial, ribosomal and cytoskeleton activity (yellow).

S15 Fig. Expression level of genes of interest in the different DS models. Different panels to show the expression level of genes of interest located or not in the region homologous to Hsa21. Data are presented as boxplot plots of th ratio of trisomic on disomic with the median and quartiles (Stastitical analysis was done comparing wt and mutant value with a student t test, * $p<0.05$, ** $p<0.01$, *** $p<0.001$).

S16 Fig. Detection of RHOA and the phoshorylated form of Myosin Light Chain (P-MLC) by Western blot in Dp1Yey hippocampal lysates and their control (wt) littermates. (A) Western blot of RHOA showed no changes in RHOA protein levels in the Dp1Yey line compared to their wt littermates (wt (n=5) and Dp1Yey (n=5)). (B) Western blot of P-MLC revealed a statistically significant decrease (* $p < 0.05$) in the amount of this protein in Dp1Yey mice (wt (n=5) and Dp1Yey (n=5)) (Student's t-test: wt vs. Dp1Yey $t(8) = 2,392$; $p = 0,0437$).

S1 Table: Summary of behavioural results including statistical assessment.

S2 Table. Volumes of each brain structure (in mm3) normalized by total brain volume derived from MRI region-based analysis.

S3 Table. Summary of the DEA and DFA results for each trisomic DS model. We included the number of trisomic genes with compensated or partially compensated expression levels, approximately half of the trisomic genes are compensated and the overall identity of DEGs are different between the models.

S4 Table. Fold-change of the gene expression in trisomic (Tg) compared to the controls for each mouse model dataset. The genes included on thoses lists were used to produce the S6 and S7 figs as follows: i) genes included inside the duplicated genomic regions of chr 16, ii) genes included inside the Ts65Dn chr17 duplicated region iii) genes of the centromeric region of chr17.

S5 Table. Pathways identified by GAGE as dysregulated including the genes contributing to each altered pathway per each mouse model multi group combination and including the name of the meta-pathway assignated.